INVESTIGATION OF THE PHOTOCATALYTIC LITHOGRAPHIC DEPOSITION OF METALS IN SEALED MICROFLUIDIC DEVICES ON TiO_2 SURFACES

A Dissertation

by

EDWARD THOMAS CASTELLANA

Submitted to the Office of Graduate Studies of
Texas A&M University
in partial fulfillment of the requirements for the degree of

DOCTOR OF PHILOSOPHY

December 2005

Major Subject: Chemistry

INVESTIGATION OF THE PHOTOCATALYTIC LITHOGRAPHIC DEPOSITION OF METALS IN SEALED MICROFLUIDIC DEVICES ON TiO_2 SURFACES

A Dissertation

by

EDWARD THOMAS CASTELLANA

Submitted to the office of graduate studies of
Texas A&M University
in partial fulfillment of the requirements for the degree of

DOCTOR OF PHILOSOPHY

Approved by:

Chair of Committee,	Paul S. Cremer
Committee Members,	David H. Russell
	D. Wayne Goodman
	Zhengdong Cheng
Head of Department,	Emile A. Schweikert

December 2005

Major Subject: Chemistry

ABSTRACT

Investigation of the Photocatalytic Lithographic Deposition of Metals in Sealed Microfluidic Devices on TiO_2 Surfaces.

(December 2005)

Edward Thomas Castellana, B.S., State University of New York College at Fredonia

Chair of Advisory Committee: Dr. Paul S. Cremer

The research presented within this dissertation explores the photocatalytic deposition of metal carried out within sealed microfluidic channels. Micro scale patterning of metals inside sealed microchannels is investigated as well as nanoscale control over the surface morphology of the nanoparticles making up the patterns. This is achieved by controlling solution conditions during deposition. Finally, the nanoparticle patterns are used in fabricating a sensor device, which demonstrates the ability to address multiple patches within a sealed channel with different surface chemistries.

Also presented here is the construction of the first epifluorescence/total internal reflection macroscope. Its ability to carry out high numerical aperture imaging of large arrays of solid supported phospholipid bilayers is explored. For this, three experiments are carried out. First, imaging of a 63 element array where every other box contains a different bilayer is preformed, demonstrating the ability to address large scale arrays by hand. Next, a protein binding experiment is preformed using two different arrays of increasing ligand density on the same chip. Finally, a two-dimensional array of mixed

fluorescent dyes contained within solid supported lipid bilayers is imaged illustrating the ability of the instrument to acquire fluorescent resonance energy transfer data.

Additionally, the design and fabrication of an improved array chip and addressing method is presented. Using this new array chip and addressing method in conjunction with the epifluorescence/total internal reflection macroscope should provide an efficient platform for high throughput screening of important biological processes which occur at the surfaces of cell membranes.

I would like to dedicate this dissertation to my parents,

Thomas and Joan Castellana,

thank you for all your love and support over the years.

ACKNOWLEDGMENTS

I would like to first acknowledge my advisor, Dr. Paul Cremer, for his advice and support throughout my graduate carrier. I also thank my committee for their support and time contribution. I would also like to thank the entire Cremer group, especially Dr. Tinglu Yang and Fernando Albertorio for all their support and advice throughout the years. Last, but definitely not least, I would like to acknowledge the assistance of the A&M Chemistry Department machinists Ken Greer and Tony Montalbano.

TABLE OF CONTENTS

CHAPTER Page

LIST OF FIGURES

FIGURE Page

FIGURE Page

FIGURE Page

CHAPTER I

INTRODUCTION

1.1 Phospholipid Bilayers

Phospholipid monolayers and bilayers closely resemble cell membranes in some key respects. These systems maintain the fluidity of their associated ligands and can be an excellent environment for presenting membrane proteins. This allows for the investigation of biological processes that occur at the cellular level, providing information about ligand-receptor interactions,[1-4] viral attack,[5,6] and cellular signaling events.[7-9]

In the 1960's Mueller *et al.* developed the first system for the investigation of the electrical properties of a planar phospholipid membrane.[10,11] The system consisted of a black lipid membrane painted over a 1 mm hole between two solution chambers. Twenty years later Tamm and McConnell developed solid supported phospholipid bilayers.[12] In 1997 Boxer *et al.* pioneered the partitioning of supported phospholipid bilayers into lithographically patterned corrals.[13] This led to the development of individually addressed arrays of solid supported phospholipid bilayers by Cremer and Yang[14] and sensor arrays for the study of cell adhesion by Groves, *et al.*[15]

This dissertation follows the style and format of the *Journal of the American Chemical Society.*

Cell surface mimicking phospholipid membranes have also been combined with microfluidic systems for the development of powerful sensor applications. Examples include on-chip immunoassays for investigating the kinetics and thermodynamics of antibody binding to antigens presented on phospholipid bilayers contained within the microchannels,[3,4] as well as bilayer coated microchannels which were used to present immobilized enzymes for rapid determination of enzyme kinetics.[16] The utility of laminar flow within microchannels has also been used to facilitate the patterning of lipid bilayer arrays within microfluidic systems.[17,18]

In certain instances black lipid membranes and vesicles have an advantage over solid supported phospholipid bilayers. For example, they avoid direct contact with an underlying substrate that can potentially be problematic for the presentation of transmembrane proteins. They also allow solution phase access to both sides of the membrane. However, they are less stable than supported membranes, harder to manipulate chemically, and are far less accessible to surface specific detection techniques. Therefore, it would be desirable to develop methods to appropriately embed transmembrane proteins into supported bilayers. To this end, Spinke et al. laid the foundation for polymer supported phospholipid bilayers on planar solid substrates.[19] It was found that thin polymer films could couple bilayers with a larger variety of materials such as metal films, oxides, and semiconductor electrodes. Adding a polymer layer between an underlying substrate and the phospholipid bilayer can be achieved by the use of either a cushioning polymer film[20-24] or the direct tethering of the membrane to a lipid presenting polymer or peptide layer.[25-30] Other effective surface modification

strategies include self-assembled monolayers (SAMs)[31,32] and the use of adsorbed or bound proteins as a cushioning layer.[33-38] To this day, however, there is not yet a completely satisfactory supported membrane system for the presentation of transmembrane proteins with both large extracellular and intracellular peripheral domains.

Supported Lipid Membranes

There are a variety of phospholipid membrane systems, supports, and detection schemes that can accommodate a host of applications. When making a choice of membrane platform, it is necessary to consider the analyte of interest. For example, simple bilayers supported on glass substrates are often sufficient for presenting small ligands for the study of multivalent interactions with extracellular proteins. On the other hand, if one wishes to incorporate transmembrane proteins or pore-forming toxins into the bilayer, it may be necessary to use a polymer-cushioned bilayer or a black lipid membrane to prevent protein denaturation on the underlying substrate. Almost equally important is the detection scheme. A conducting substrate is required if the sensor design calls for a direct electrical measurement. In this case the bilayer can be supported on an indium-tin-oxide (ITO) electrode or even a gold electrode if an appropriately hydrophilic alkanethiol monolayer is employed. A good review of phospholipid membranes on solid surfaces is reference.[39]

Black Lipid Membranes

The black lipid membrane derives its name from its appearance by optical microscopy. When Mueller *et al.* observed the formation of the first black lipid membranes[10,11] from extracted brain lipids, they noted interference bands giving rise to color in the membrane. This interference effect disappeared during the thinning of the painted lipid mass and is thought to indicate the formation of a single bilayer membrane. For an excellent resource on black lipid membranes see reference.[40]

Several methods of producing black lipid membranes exist. All involve the formation of a membrane over a small aperture usually less then 1 mm in diameter. The hole is formed in a hydrophobic material such as polyethylene or Teflon and is usually part of a wall separating two compartments that can be filled with aqueous solution, each containing a reference electrode. Two of the most popular methods of BLM formation involve the painting of the lipid solution over the aperture[10] and the formation of a folded bilayer.[41] The result of either method is a bilayer suspended over the aperture with an aqueous compartment on each side of it.

The painting of a black lipid membrane is carried out with a small artist paint brush. Typically a 1-2% phospholipid solution in an organic solvent, such as n-decane or squalene, is painted across the hole under an aqueous solution. The deposited lipid mass thins as it spreads, forming the black lipid membrane. This methodology has remained basically unchanged over the decades.[10] The formation of folded lipid bilayers requires a cell with two compartments separated by a small aperture and the solution levels in each compartment must be controlled independently. Both compartments are

filled with the desired aqueous solution and a monolayer of phospholipid material is spread on top of one of the compartments. The solution level in the compartment containing the lipid monolayer is slowly lowered below the aperture and raised again. This deposits a monolayer on each pass to form the completed bilayer membrane.[41]

Since their advent, black lipid membranes have been used to investigate various biophysical membrane facilitated processes. One of the most important is the formation of ion channels in phospholipid bilayers by peptides,[42] proteins,[43,44] antibiotics,[45] and other pore forming biomolecules. Of particular interest for creating nanodevices is the insertion of single protein pores for use as stochastic sensors. This has been accomplished by Gu *et al.* through the use of genetically modified α-haemolysin.[46] Naturally occurring α-haemolysin, which is composed of seven identical subunits, is an exotoxin produced by *Staphylococcus aureus* bacteria.[47] Through the use of genetic modification, an α-haemolysin mutant was created which can non-covalently capture a cyclodextrin molecule within its pore. A current change at fixed voltage is measured when the cyclodextrin inserts into the channel due to a restriction of the pore cross-section. The current is further attenuated by the binding of a guest molecule in the cyclodextrin binding pocket. The binding and unbinding of small organic molecules within the cyclodextrin/α-haemolysin pore can ultimately be measured at the single molecule level via this process.[46]

This same methodology has been applied to the stochastic sensing of divalent metal cations[48] and cell signaling molecules.[49] Polyhistidine motifs are known to strongly interact with divalent cations and are often employed in the purification of

recombinant proteins. Pores designed to stochastically detect divalent metal cations were genetically engineered to present a short peptide sequence of four histidines inside the α-haemolysin pore.[50] A similar approach was used in the detection of cell signaling molecules. Pores were engineered with a ring of 14 arginine residues on their inside surface. It was shown that the phosphate groups on inositol 1,4,5-trisphosphate, a second messenger, interact with the ring of arginines, effectively blocking the pore.[49]

Current measurements across a modified α-haemolysin pore show that the frequency of binding events relates to the concentration of the analyte. The amplitude of the current change together with the duration of time an analyte spends in the channel allows for specific identification of a given species.[51] Since only one molecule can fit into the channel at a time, analyte identification can be preformed for individual blocking events. This means that the same pore can be used in a sequential fashion to detect a variety of analytes.

As noted above, black lipid membranes are suspended in solution and there are no unwanted interferences of the membrane with an underlying support. The absence of such a support also means that transmembrane proteins suspended within the phospholipid bilayer remain fully mobile and active. However, this also limits the lifetime of the bilayer due to poor stability of the membrane. The methods of detection that can be employed with black lipid membranes are also typically limited. Usually electrical conduction and simple light microscopy are used; however, more recently investigators have begun to utilize more sophisticated optical techniques.[40]

Solid Supported Lipid Bilayers

Phospholipid bilayers supported by solid substrates are more robust and stable than black lipid membranes. Solid supports also open the door for the use of surface specific analytical techniques not available for black lipid membranes. In solid supported systems membrane fluidity is maintained by a thin 10-20 Å layer of trapped water between the substrate and the bilayer.[12,52] A schematic diagram of a supported lipid bilayer is shown in Figure 1.1.

The varieties of substrates capable of supporting phospholipid bilayers are somewhat limited. In order to support a high quality membrane (i.e. little or no defects and high lipid mobility) the surface should be hydrophilic, smooth, and clean. The best substrates for supporting phospholipid bilayers are fussed silica,[12,53] borosilicate glass,[12,54] mica,[55,56] and oxidized silicon.[12] Bilayers can also be formed on polished single crystals of TiO_2, $SrTiO_2$,[57] and thin films of SiO_2 on $LiNbO_3$ crystals.[58] Thin films can be used as solid supports as observed with TiO_2,[59-61] indium tin oxide,[62,63] gold,[64,65] silver,[66] and platinum.[67]

There are three general methods for the formation of supported phospholipid bilayers on planar supports for sensor applications. The traditional method involves the transfer of a lower leaflet of lipids from an air-water interface by the Langmuir-Blodgett technique. This is followed by the transfer of an upper leaflet by the Langmuir-Schaefer procedure, which involves horizontally dipping the substrate to create the second layer.[12] A second method of supported bilayer formation is the adsorption and fusion of vesicles from an aqueous suspension to the substrate surface.[68,69] Also, a combination of the two

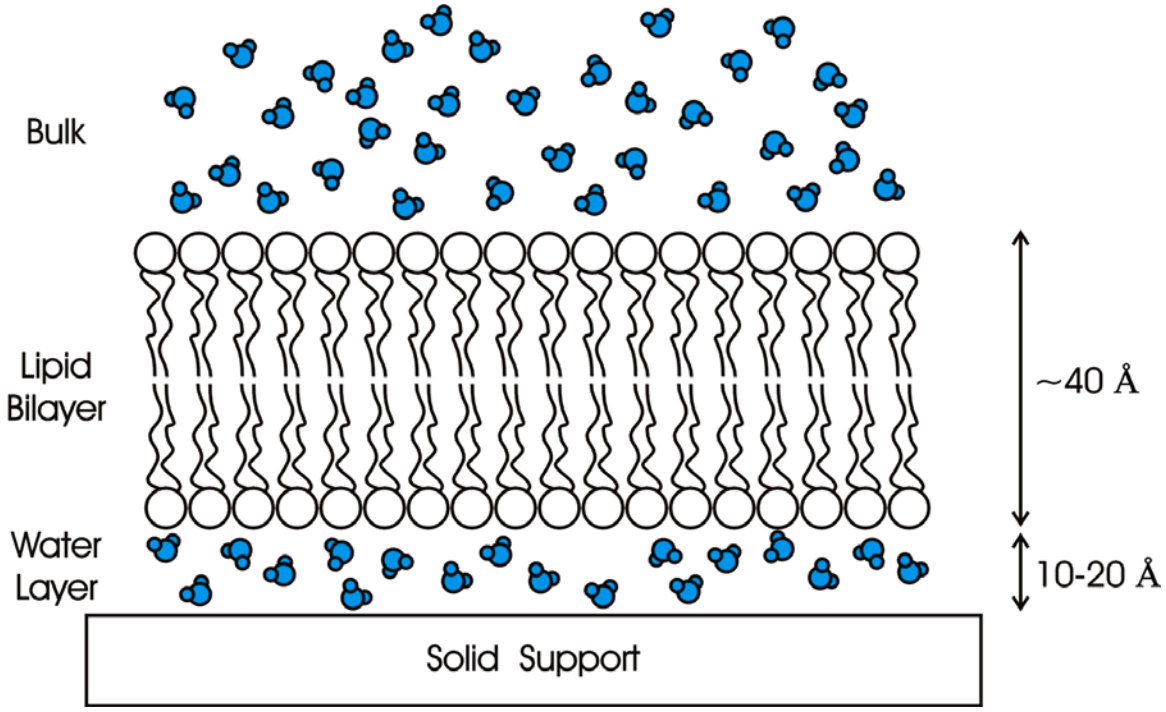

Figure 1.1. Schematic diagram of a solid supported phospholipid bilayer. The membrane is separated from the substrate by a 10-20 Å lubricating water layer.

methods can be employed by first transferring a monolayer via the Langmuir-Blodgett technique followed by vesicle fusion to form the upper layer.[70] Each method has its particular advantages and disadvantages.

The transfer of amphiphilic molecules from the air-water interface to a solid substrate dates back to the 1920's.[71] An excellent review of this topic is found in reference.[72] Tamm and McConnell were the first to apply this technology to form supported phospholipid bilayers by sequential monolayer transfer onto quartz, glass, and oxidized silicon substrates.[12] This method is excellent for the formation of asymmetric bilayers;[61] however, it is difficult or impossible to incorporate transmembrane proteins into the membrane with this technique because prior to transfer portions of the proteins within the monolayer are exposed to air and can become irreversibly denatured.[70]

The adsorption and fusion of small unilaminar vesicles (SUVs) is one of the easiest and most versatile means for forming solid supported phospholipid bilayers. SUVs can be prepared by a multitude of methods. The simplest involves the extrusion of multilaminar vesicles through porous polycarbonate membranes at high pressure.[73-76] Another method is the sonication and ultracentrifugation of aqueous lipid suspensions.[77] The incorporation of transmembrane proteins into SUVs requires a gentler process such as detergent removal via dialysis.[78,79] Factors effecting the adsorption and fusion of SUVs to solid supports include: the vesicle composition, size, surface charge, surface roughness, surface cleanliness, solution pH, ionic strength, and osmotic pressure of the vesicles.[59,80] The process begins with the adsorption of vesicles from the bulk solution onto the substrate. In the early stages, SUVs adsorb and fuse with one another. Once a

critical size is reached, the vesicles will begin to rupture and fuse to the substrate forming planar supported bilayers.[80] The adsorption process can be accelerated by the presence of divalent cations such Ca^{2+} and Mg^{2+}.[61] Fusion of SUVs to the substrate can also be enhanced by heating,[63] creating an osmotic gradients across the vesicle membrane,[59] and by the addition of fusigenic agents such as polyethylene glycol.[36]

A combination of Langmuir-Blodgett monolayer transfer and vesicle fusion can also be used to form supported phospholipid bilayers.[70] This method involves the fusion of SUVs to a predeposited monolayer of phospholipid. It is also useful for the formation of asymmetric bilayers and for the incorporation of transmembrane proteins into solid supported bilayers.[70]

It is well established that phospholipid membranes are held in place above a solid oxide support by a combination of van der Waals, electrostatic, hydration and steric forces.[54] In an egg phosphatidylcholine (egg-PC) bilayer supported on a glass substrate, the underlying water layer effectively lubricates the lipids, which allows them to freely move with a diffusion constant of approximately 4 $\mu m^2/s$.[81] Furthermore, it has been observed that negatively charged vesicles do not easily fuse to glass substrates at basic pH values and low ionic strengths.[54] This demonstrates the delicate balance of forces involved in bilayer fusion and spreading.

The main advantage in using solid supports is clearly an increase in robustness and stability of the phospholipid bilayer membrane. Almost equally important is the ability to probe interactions that occur at the membrane surface with powerful analytical techniques that are surface specific. While solid supported phospholipid bilayers are

somewhat limited in terms of their substrate compatibility, their major disadvantage is that the supported membrane is not truly decoupled from the underlying substrate. Indeed, the system may not prevent transmembrane proteins from interacting unfavorably with the underlying substrate. Such interactions with the surface can cause proteins in the membrane to become immobile and hinder their function.

SAM/monolayer Systems

The use of self-assembly for the modification of electrode surfaces has been the topic of several reviews.[82-84] This includes the use alkanethiols to form self-assembled monolayers (SAMs) on gold and other widely used electrode surfaces such as silver and mercury. Methyl-terminated alkanethiols on gold provide a well-defined hydrophobic surface to facilitate the formation of a hybrid bilayer membrane for use as a cell membrane mimic.[1,31,85] In its simplest form, the hybrid bilayer membrane consists of a metal supported alkanethiol SAM and a monolayer of phospholipid as illustrated in Figure 1.2.[86]

There are a plethora of alkanethiols which will self-assemble on a gold surface either as a pure substance or in mixtures. Octadecanethiol is a typical choice for hybrid bilayer formation due to its ability to form tightly packed well-ordered monolayers. The SAM layer can be formed by incubating a clean gold substrate with a 1 mM alkanethiol solution in ethanol for a minimum of 12 hours.[86] Another formation method involves Langmuir-Blodgett transfer.[87] Two general methods exist for applying the phospholipid leaflet to the SAM covered surface: vesicle fusion and lipid transfer from an air-water

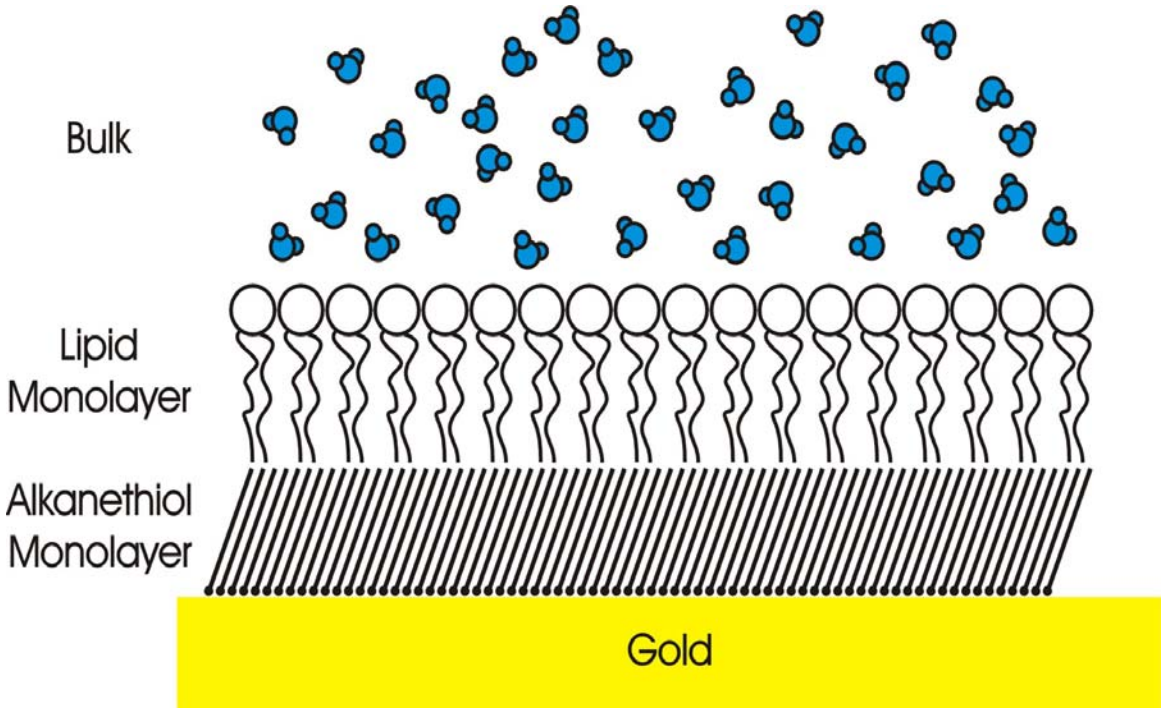

Figure 1.2. Schematic illustration of a hybrid bilayer. A single phospholipid monolayer rides on an alkanethiol SAM.

interface by the Langmuir-Schaefer method.[88] Vesicles in aqueous buffer have been shown to spontaneously fuse to the hydrophobic surface of supported lipid monolayers[70] and alkanethiol SAMs.[31] The process of vesicle fusion to such surfaces has been investigated by surface plasmon resonance,[89] cyclic voltammetry, and impedance spectroscopy.[90] Alternatively, a phospholipid monolayer can be transferred from the air-water interface to the hydrophobic surface of an alkanethiol SAM.[91] This method requires a horizontal transfer from a stable phospholipid monolayer supported in a Langmuir trough at the air/water interface.

The fusion of ghost cells to alkanethiol SAMs also produces a hybrid bilayer membrane.[85,87,89] Ghost cell fusion offers the ability to reconstitute some of the contents of a cell membrane onto a sensor platform. Such a procedure may eventually represent an efficient means of presenting biomimetic surfaces containing natural mixtures of proteins, lipids, and receptors, as well as cellular membranes from genetically modified cells. It is not clear, however, how transmembrane proteins interact with such surfaces since these species cannot intercalate beyond the alkanethiol SAM.

The physical properties of the membrane can be altered through the use of different alkanethiols, lipids, and membrane additives such as sterols and proteins. For example, increasing the chain length of the alkanethiol or phospholipid results in a thicker membrane, thus decreasing it's capacitance.[31,92] Altering the composition of the vesicles used to form the lipid layer can also change the properties of hybrid membranes. Incorporation of ligand presenting phospholipids into bilayer membranes is useful for investigations of binding kinetics and multivalent interactions. In this respect, hybrid

bilayer formation from the fusion of phospholipid vesicles containing ligand presenting phospholipids has been shown to be effective.[1,93]

The underlying SAM layer must be only slightly modified to accommodate membrane active peptides and transmembrane proteins with small or nonexistent peripheral domains facing the electrode. This can be accomplished through the introduction of ethylene oxide spacer units at the base of the alkanethiol.[94] Examples of proteins that can be investigated in this manner include α-hemolysin and melittin. These proteins alter the electrical properties of membranes,[94] but barely protrude beyond the membrane on the distal side. This has allowed neutron reflectometry investigations[95] to be carried out to determine the orientation of melittin within this lipophilic system. Melittin has also been investigated by cyclic voltammetry in this manner.[31,92]

There are several advantages to choosing hybrid phospholipid platforms for sensor applications. Foremost is the coupling of the cell surface mimicking phospholipid monolayer directly to a metallic surface. This allows for non-labeled analyte detection by such means as direct electrical measurements, surface plasmon resonance, and quartz crystal microbalance detection. Hybrid phospholipid membranes are often more robust than their solid supported counterparts due to the strong interaction between the alkanethiol SAM layer and the underlying substrate. When formed at an air-water interface, they can be dried and rehydrated while retaining at least some of their original physical and chemical properties.[91]

While the rigidity and close packing of the underlying alkanethiol SAM layer provides many advantages, it also presents several limitations. An alkanethiol SAM

layer is more crystalline in structure[94] than a normal leaflet of a phospholipid bilayer. This results in a less fluid membrane environment. Insertion of proteins is also effected by the packing density of the underlying SAM layer,[94] which can inhibit proper functioning. Of course, transmembrane proteins with both large extracellular and intracellular domains cannot be inserted in a hybrid bilayer.

Polymer Cushioned Lipid Bilayers

While solid supported phospholipid bilayers and hybrid bilayers are excellent sensor platforms for the investigation of cellular processes that occur at the membrane/solution interface or within the membrane itself, they have difficulty mimicking a natural fluid environment for many transmembrane proteins, especially those presenting large peripheral domains.[96] The 10-20 Å water layer that resides between a phospholipid bilayer and a solid support provides lubrication and maintains sufficient mobility for the lipid molecules;[12,52] however, the underlying water does not protect peripheral portions of transmembrane proteins from immobilization or denaturation if they come in contact with the substrate. Figure 1.3 illustrates the protection of a transmembrane protein by a lipopolymer support.[97] The desire to mimic complex fluid biological systems has been the driving force for the development of polymer supported phospholipid bilayers.[96]

The addition of a polymer layer effectively decouples the membrane from the surface and still allows for investigation by such surface specific techniques as neutron reflectivity, surface plasmon resonance, total internal reflection fluorescence

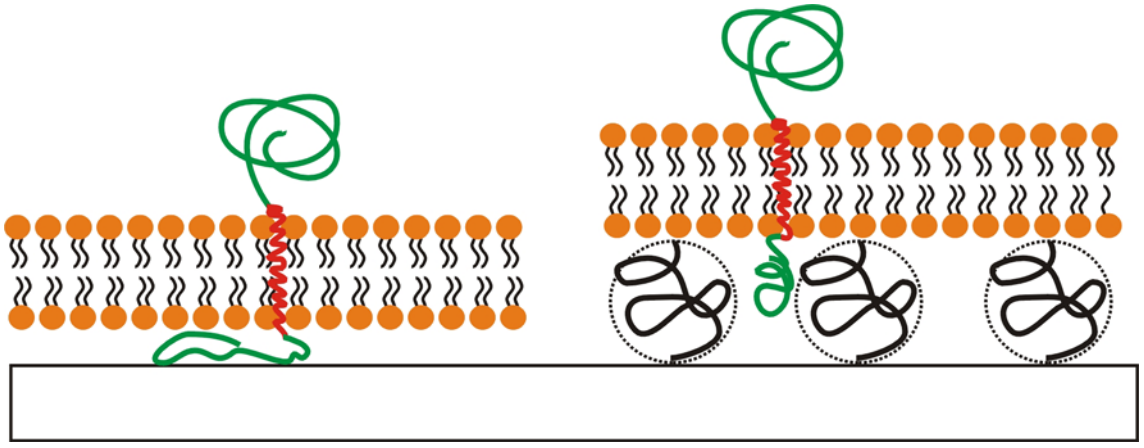

Figure 1.3. Comparing solid to polymer supports for phospholipid bilayers. On the right, periphery domains of transmembrane proteins can become immobilized and denatured on a solid support. On the left, a polymer cushion shields the protein from the substrate and maintains its mobility within the bilayer.

microscopy, fluorescence interference-contrast microscopy, and attenuated total reflectance Fourier transform infrared spectroscopy. In principle these systems should always prevent nonspecific adsorption of transmembrane proteins that have been reconstituted into a phospholipid membrane. Another potential advantage of the polymer support is the ability to avoid nonspecific adsorption from solution that can occur at defect sites in solid supported bilayers lacking polymer cushions. Large numbers of such defect sites contribute to poor sensitivity and low signal-to-noise ratios especially in electrical detection schemes where electron or ion transport to and from the substrate is monitored.[60]

In erythrocyte cells, the cellular membrane is supported by the cytoskeleton, a protein matrix, which supports the lipid membrane and gives the cell shape. A well designed polymer cushion should behave much like a cytoskeleton. The design of systems for the support of phospholipid bilayers requires careful consideration of the balancing of surface forces.[20] In physisorbed systems, too much or too little interaction between the phospholipid bilayer and the polymer support will result in an unstable system. This may be overcome by covalent attachment of the polymer layer to the substrate. It is also useful to use anchor lipids or alkyl side chains capable of inserting into the phospholipid bilayer, effectively tethering it to the underlying polymer layer. In general, it is desirable for the polymer support to be soft, hydrophilic, not highly charged, and not extensively cross-linked.[20]

There are several types of polymer cushions that have been explored for supporting phospholipid bilayers. These include dextran,[23] cellulose,[98] chitosan,[24]

polyelectrolytes,[21,99-101] and lipopolymer tethers.[19,22,25,26,29,30,97] Two classes of polymer, polyelectrolytes and lipopolymers, are emerging as the most popular choices for cushion material. Polyelectrolyte cushions represent a highly versatile support for phospholipid bilayer membranes. They can be adsorbed to a variety of substrates by means of layer-by-layer deposition, providing a great deal of control over the resulting film thickness. Polyethylenimine (PEI) has been used to support phospholipid bilayers on mica[102] and quartz.[96,99] On metallic substrates such as gold, polyelectrolytes can be adsorbed to charged SAMs. Mercaptoundecanoic acid on gold is capable of adsorbing alternating layers of polydiallyldimethylammonium chloride (PDDA) and polystyrene sulfonate sodium salt (PSS) for use as a polymer cushion.[21,100]

Polyelectrolyte cushions rely on electrostatic interactions to balance the necessary forces required to hold the system together. Here, alternating charges are the key. Electrostatic attraction between the substrate and polymer cushion binds the polymer layer to the substrate. In turn, van der Waals, hydrogen bonding, as well as electrostatic interactions bond the lipid layer to the polymer. When a polyelectrolyte layer is deposited onto a substrate, charge on the surface builds up repelling excess material away from the surface. Under appropriate conditions this results in highly uniform films with a linear relationship between thickness and the number of adsorbed layers.[103] This is of course advantageous for assembly of supported bilayers. On the other hand, the necessity of electrostatic charges to keep polyelectrolyte cushions in place presents certain limitations. Too much charge can adversely affect the function and mobility of membrane constituents and alter interactions between proteins and the

supporting cushion. The strength of the attractive forces is also directly affected by the solution environment; namely ionic strength and pH. This can be problematic, as important biological processes occur in different solution environments.

Lipopolymers are another class of highly effective polymer cushions. They consist of a soft hydrophilic polymer layer presenting lipid like molecules at their surface which can insert into a phospholipid membrane and tether it to the polymer spacer. Tethering has the advantage of being much less affected by solution conditions such as pH and ionic strength. However, a large degree of tethering can interfere with the mobility of the individual components within the supported membrane.[27]

Often lipopolymers are also covalently bonded to the substrate. This provides additional support for the membrane system. Attachment of a lipopolymer to a substrate has been carried out via photoreactive coupling,[22,23,27] sulfur-metal bond formation ,[26,28,29] epoxy group linkage,[23] or silane bonding.[97] Some common polymer backbones used in the synthesis of lipopolymers are, acrylamide,[19,26,29] ethyloxazoline,[22,27] and ethyleneglycol .[97] It is important that the polymer cushion have the ability to swell in an aqueous environment and have minimal disruptive interactions with the bilayer and reconstituted membrane components.[20] The degree to which a polymer cushion swells in an aqueous humid environment is a good indication of its ability to be employed as a support. It has also been observed that the quality of the supported membrane can be affected by the degree of swelling of the polymer layer prior to bilayer deposition.[96] Swelling is typically monitored in a home-built humidity chamber and can easily be detected with ellipsometry [23] or surface plasmon resonance spectroscopy.[22]

Lipopolymers can be synthesized prior to adsorption onto a substrate or built up on a support by polymer grafting techniques. The lipid tethers are typically attached during polymer synthesis or by reacting specific lipids within a Langmuir-Blodgett transferred monolayer with active sites on the polymer.[25] Lipids presenting a succinimide headgroup are a convenient means for attaching tethers to amino groups presented by a polymer support.

Bilayer formation on polymer cushions can occur by means of vesicle fusion or the Langmuir-Blodgett/Langmuir-Schaffer transfer method. Langmuir-Blodgett transfer of mixed monolayers of phospholipids and lipopolymers from an air/water interface has been shown to provide excellent control over the density of the lipopolymer cushion layer.[27,97] It has also been observed that protein containing vesicles fusing to these deposited monolayers can result in highly oriented transmembrane proteins in the supported bilayer.[104] If the transmembrane protein has peripheral domains that are only presented on only one side of the cellular membrane, such domains sometimes prefer to orient into the bulk solution.

Another advantage of using lipopolymers is the ability to form air stable supported lipid bilayers.[105] Through vesicle fusion of phospholipid vesicles containing small amounts (less than 5 mole percent) poly(ethylene glycol) conjugated lipids it is possible to form a polymer cushioned bilayer. This bilayer has the added advantage of an added layer of lipopolymer in the upper leaflet of the bilayer, which has been shown to protect the phospholipid bilayer upon exposure to air and re-hydration. It is also noted that the presence of this polymer layer still allows for the binding of proteins to

ligands presented at the surface of the bilayer but inhibits the interaction of micron sized particles with the membrane.[105]

It should be noted that some polymer supports have been shown to exhibit less than desirable effects on the supported membrane. An imbalance in the stabilization forces or a large number of tethering molecules can decrease the mobility of the supported phospholipid bilayer and alter the phase transition temperature. In some cases, a polymer supported phospholipid membrane is less stable than one formed directly on a solid support and can even possess a larger number of defects.[20]

1.2. Titanium Dioxide

Titanium dioxide (TiO_2) is a widely used material in everyday society. It is found in products ranging from paint and crayons to food coloring, cosmetics and sunscreens. Its photocatalytic ability allows it to be utilized in self cleaning products such as tiles, windows, and lamp coverings. It can be utilized to purify water for drinking and environmental cleanup and air in buildings and for food storage applications. Its self sterilizing capabilities make it a useful coating for hospital facilities and equipment. An interesting property of TiO_2 is its ability to exhibit superhydrophilicity. This is achieved in mixed films with the proper ratio of by of TiO_2 to SiO_2.

Production of TiO_2

Several methods exist for the production of photoactive TiO_2. The main techniques are through the chloride method[106], sol-gel processing,[107-109] and chemical vapor deposition (CVD).[110] The sol gel process is the most common method and can be used to produce both particulate and thin film TiO_2 through the hydrolysis of a titanium metal alkoxide. The alkoxide is typically dissolved in an alcohol solvent and mixed with water, which hydrolyzes the alkoxide to produce the TiO_2 sol. This sol can be coated onto substrates and gelated to form photoactive TiO_2 thin films.

The most common method of producing TiO_2 crystallites is through the thermal decomposition of $TiCl_3$ vapor, which is known as the chloride method. This is done by reacting titanium minerals with Cl_2 gas at high temperatures.[106] This is the method used to produce commercially available Degussa P-25, a widely used, photoactive TiO_2 nanocrystalline powder.

A simple room temperature, atmospheric pressure CVD was developed in our laboratory for investigating the water structure at the TiO_2 water interface.[110] This process can be used to generate photoactive TiO_2 thin films if deposition times of 30-120 min. are used. The processes involves the vapor deposition of the metal oxide precursor titanium isopropoxide onto silica substrates. Immediately following vapor deposition, the substrates are calcinated at elevated temperatures. In this study the process was expanded to be used on Pyrex wafers. Here, to insure photoactivity, acid treatment of the wafers is necessary not only to activate the surface but to remove sodium ions from the surface layers of the Pyrex.[111]

Photocatalysis

TiO_2 is a semiconductor with a bandgap of approximately 3eV. This means that photoexcitation occurs when photoactive TiO_2 is illuminated with light of a wavelength less than 400 nm. This process generates electron hole pairs within the semiconductor which can be used for oxidation and reduction reactions. The photocatalytic activity of TiO_2 is dependent upon the electron hole recombination lifetime and the surface area.[112] The higher the surface area, the greater the number of surface active sites and the slower the recombination time, the higher the probability a photogenerated electron or hole will react with an adsorbed molecule instead of with each other. Besides increasing surface area and crystallinity, the photoactivity can be increased through the addition to metal to the surface of the particles or thin films. This increase has been observed for a variety of metals such as gold,[113-116] and silver.[113,117-119] Metal loading has shown to enhance photocatalytic activity for such uses as organic synthesis,[116,119-121] water purification,[122-125] and antimicrobial properties.[126-128]

1.3. Microfluidics and Micromachining

Microfluidic technology involves the handling of fluids within devices consisting of channels on the size scale of 10-100 microns. The small size of the channels allows the user to work with sample volumes on the order of nanoliters to picoliters. This becomes advantageous when one is investigating processes involving expensive analytes such as proteins, peptides, etc. The field of microfluidics has played a pivotal role in the development of Lab-on-a-Chip and micro-total analytical systems. Such systems find

uses in; genomics and proteomics,[129-131] on-chip polymerase chain reactions,[132-136] clinical analysis,[137-141], high throughput screening,[142] ligand-receptor binding,[3,4] enzyme catalysis,[16,143,144] studying physical chemistry of proteins,[3,145-147] environmental testing,[148] medicine,[149] and single molecule detection.[150,151]

Perhaps one of the most important factors in the rise in popularity of microfluidics research is its ability to be rapidly prototyped.[152] By using soft lithography techniques it is possible to relatively inexpensively carry out microfluidic research and device design in non-cleanroom environments. This enables research in the field to be carried out by a much broader class of scientists. Some of the important micromachining concepts, which are used to develop microfluidic systems and array based platforms are discussed in the next few sections.

Photolithography and Soft Lithography

Photolithography is the process of transferring desired patterns from a mask onto a thin photoactive polymer layer (photoresist) on the surface of a substrate. The basic processes of photolithography are; substrate cleaning, photoresist application spinning, soft baking, ultraviolet (UV) exposure, developing, and sometimes hard baking. A wide variety of commercially available photoresists exist allowing for a wide range of thickness for both positive and negative resists. Thickness is easily controlled by choosing a photoresist with the appropriate viscosity and spin coating it at the proper speed.

Negative resists work through UV assisted reactions which increase the degree of polymerization and cross linking within the polymer layer. The areas which are exposed to UV radiation are much more resistant to the developing solutions and remain in place when unexposed regions are removed exposing the underlying substrate.

Positive photoresist is the opposite of negative. The polymers in the areas of the photoresist which are exposed to UV radiation are broken down. This makes the film more susceptible to chemical attack by the developing solution leaving behind only those regions of the resist film which were masked during UV exposure.

Once the pattern is transferred to the surface one can then transfer the pattern into the substrate through a variety of dry or wet etching techniques. Also, a lift of method can be used to deposit materials, such as metals, to exposed regions of the underlying substrate through a process know as lift off. After the material of choice is deposited, the photoresist is removed along with the deposited material on top of it. This leaves behind only the material deposited on the exposed regions. Alternately, the patterned photoresist can be used as a master template for soft lithography. An illustration of the photolithographic process is shown in figure 1.4.

Soft lithography is a micromachining technique which encompasses two main techniques; micromolding[152-155] and microcontact printing.[156-160] Micromolding involves the transfer of a pattern, i.e. patterned photoresist, to a soft material such as poly(dimethylsiloxane) (PDMS). Micromolded PDMS is an excellent choice for the fabrication of microchannels because it is inexpensive, optically transparent material

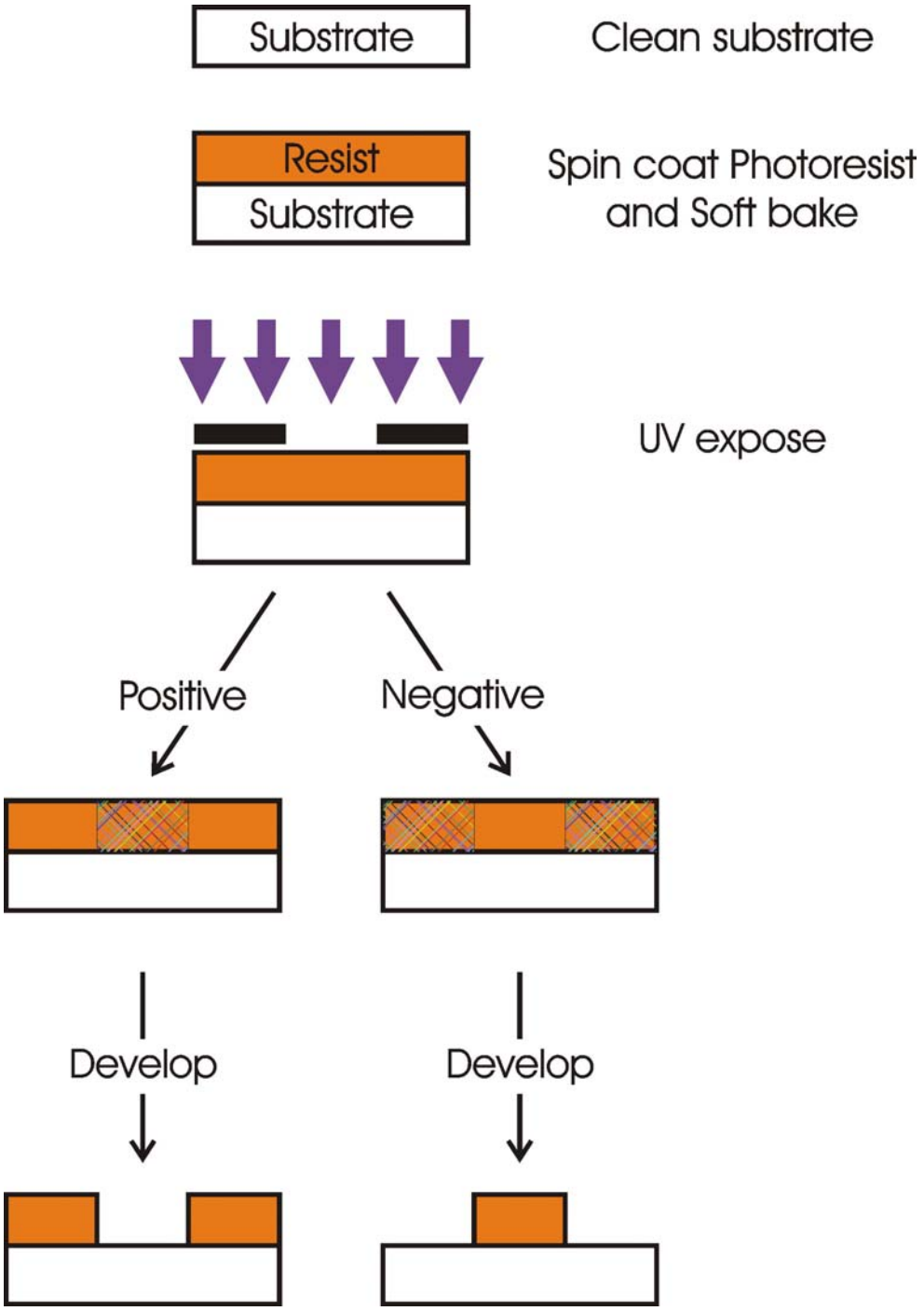

Figure 1.4. Schematic of the lithographic process.

which is easily bonded to glass through the use of an oxygen plasma.[161] It can be used with both pressure and electrokinetic driven flow systems. It is however limited to aqueous solutions and only a few organic solvents.[162] A schematic of the soft lithography process for forming microfluidic channels is shown in figure 1.5.

Wet Etching

Wet chemical etching allows for controlled etch rates and a high degree of selectivity. The etching process proceeds by transport of etchant to the exposed surface, reaction between the etchant and the surface, and transport of the reaction products away from the surface. Typically the wet etch process is rate limited by the surface reaction. This allows for a high degree of control in etch rate by simply controlling the temperature and composition of the etch bath.

The process of wet etching is generally broken down into two categories, isotropic and anisotropic. Isotropic etching removes material from the surface equally in all directions and can be carried out on any material. Isotropic etching of silicon is usually carried out with a mixture of hydrofluoric and nitric acids at elevated temperatures where isotropic etching of glass is typically carried out using a buffered hydrofluoric acid solution. Anisotropic etching requires both a material of crystalline structure and an etching solution which has different etch rates from different crystal planes within the substrate. In the case of crystalline silicon, wet etching of the silicon <100> plane is much greater then the <111> plane when etched with a potassium hydroxide solution. This makes it possible to etch deep into a silicon substrate with a

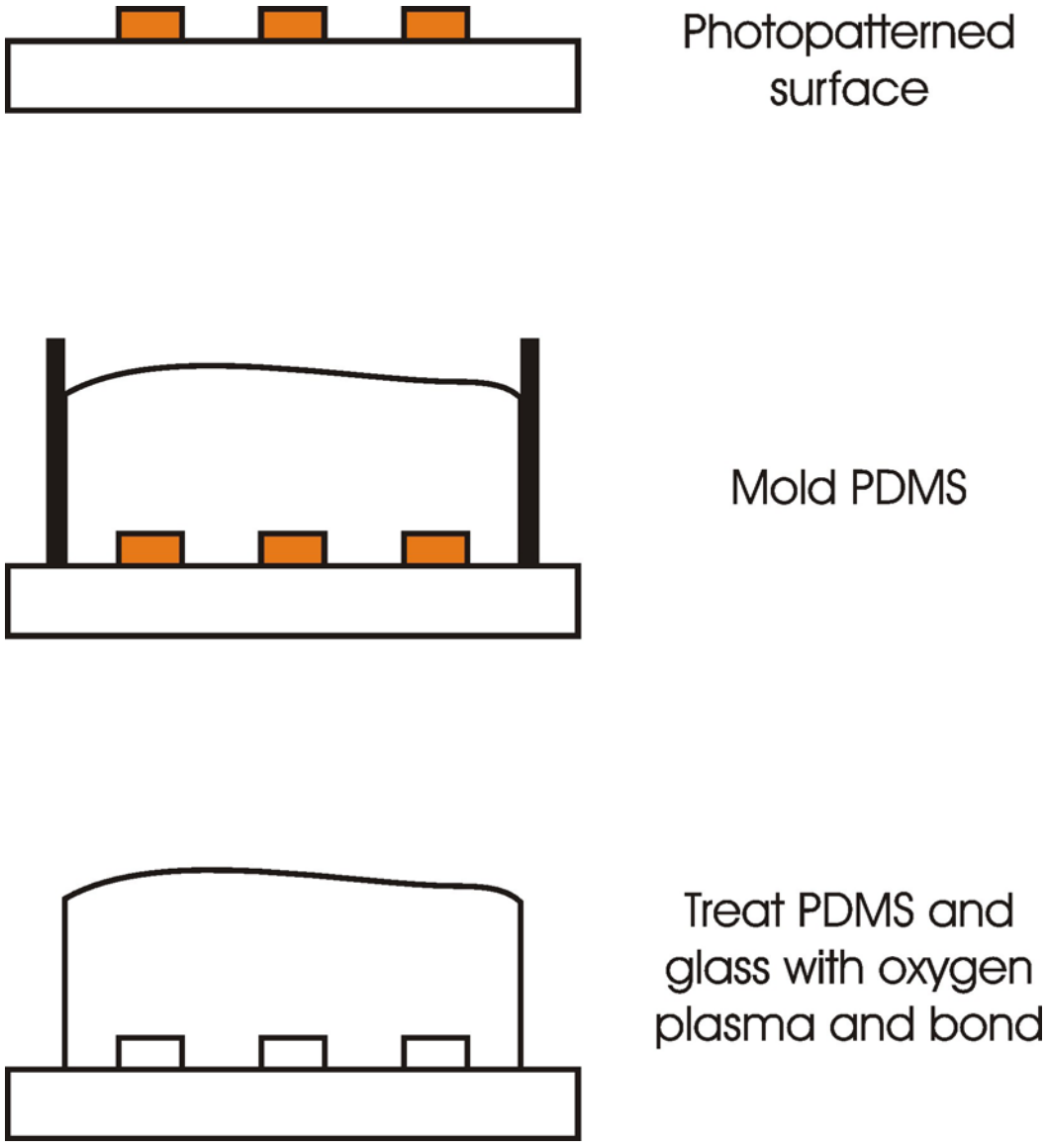

Figure 1.5. Schematic of microfluidic device fabrication using soft lithography.

relatively high aspect ratio to that of an isotropically etched feature. When etching a silicon wafer with a 40 % KOH solution at 85° C the etch rate is 1.4 microns/min and the ratio of the etch rates for <100>:<111> is approximately 400:1.[163] An illustration of anisotropic and isotropic etching is shown in figure 1.6.

Reactive Ion Etching

Reactive ion etching (RIE) is a dry etching process that is carried out in a radio frequency (RF) plasma. It involves the ionization of a reactive gas such as CF_4 or SF_6. In the presence of the RF plasma, the reactive gas is broken down into radical species some of which become ionized. These highly reactive ions can then be accelerated towards the surface of a substrate by an applied electric field. Products formed from the gas reacting with the surface are either volatized by the low pressure environment or removed from the surface due to ion bombardment. As this process proceeds, exposed areas on the surface are etched. The process is typically isotropic in nature; however, the bottoms of the etched features usually etch faster then the walls due to the higher frequency of reactive gas ions contacting the surface. In general reactive ion etching is an excellent method to pattern a hard masking material such as silicon nitride or silicon dioxide. For RIE of hard mask layers, photoresist can be used to mask the hard mask layer. A schematic of the RIE chamber is shown in figure 1.7.

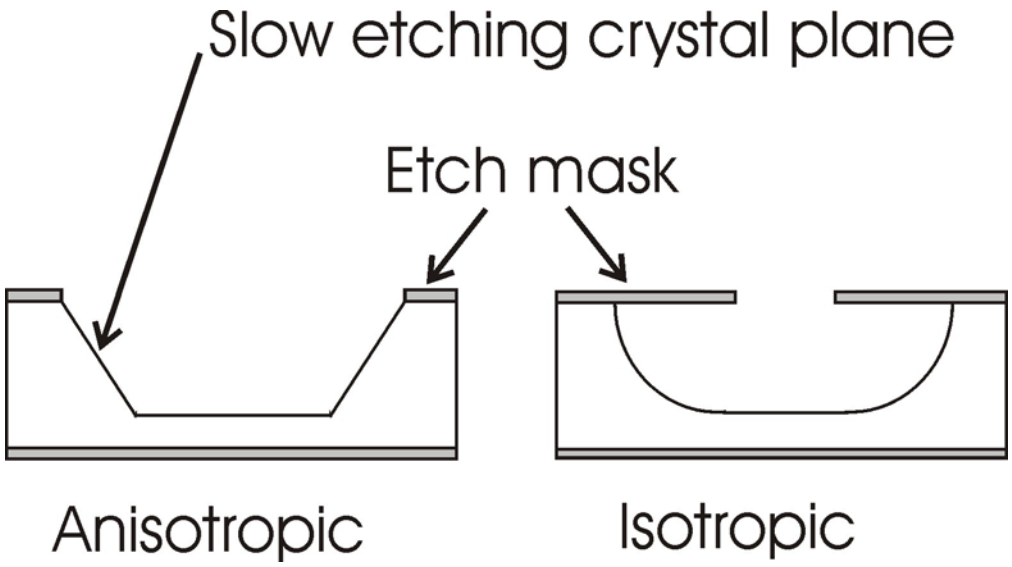

Figure 1.6. Anisotropic and isotropic etching.

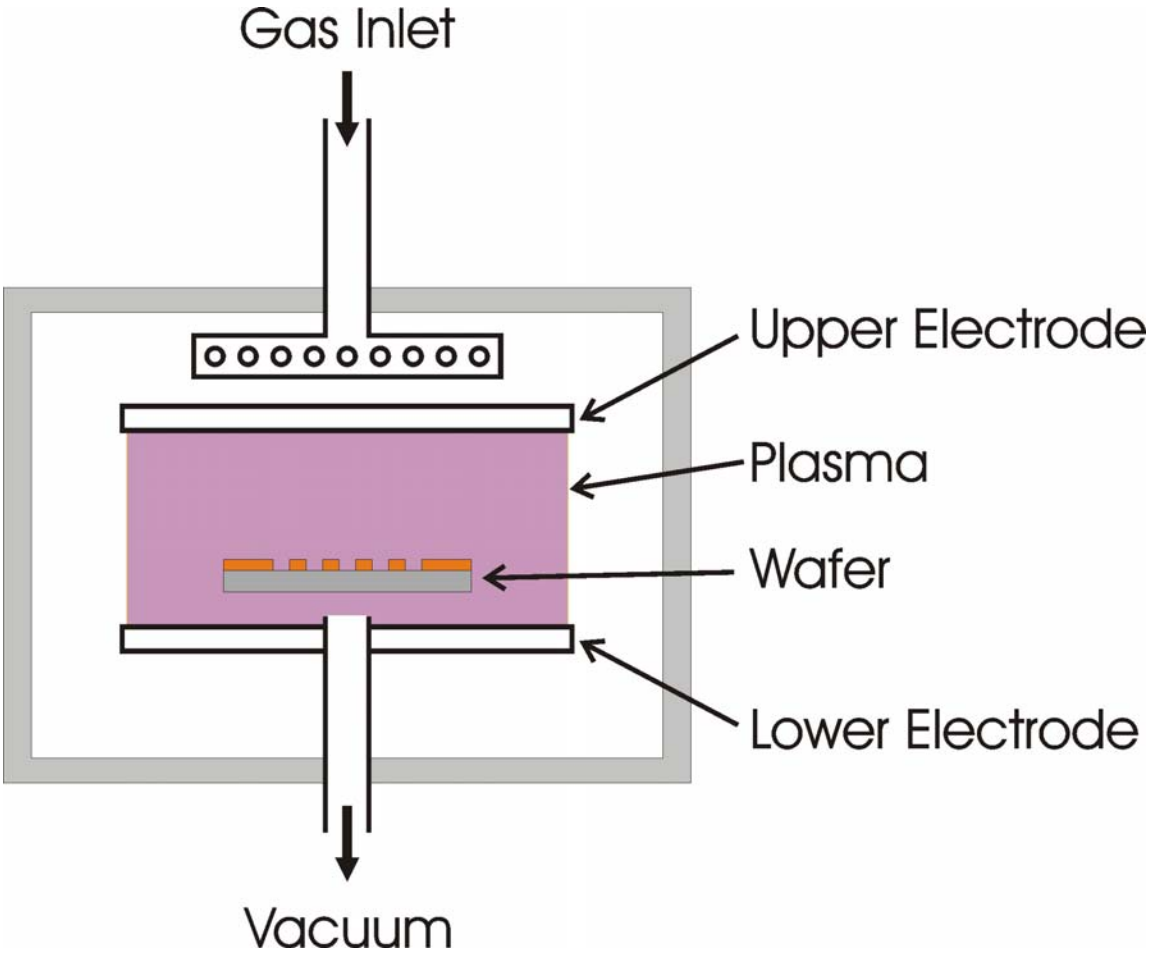

Figure 1.7. A schematic of the RIE process. A gas such as CF_4 is broken down in the plasma generating reactive ions. These ions are then accelerated towards the surface by an electrical potential between the upper and lower electrodes.

Anodic Bonding

The process of anodic bonding is used to join together glass and silicon substrates at elevated temperatures under high electrical potentials.[164] Both surfaces need to be extremely clean, free of contaminate particles and the areas where bonding is desired must be highly polished. It requires a sodium containing glass which has a similar thermal expansion to that of silicon. An excellent material for this is Pyrex 7740, which was specifically designed to have good thermal expansion match to that of silicon. The elevated temperature allows the sodium in the glass to become more mobile and drift towards the cathode under high bias. The depletion of sodium ions in the glass at the interface makes the surface of the glass highly reactive with the silicon surface forming a strong chemical bond between the two substrates. In experiments discussed later a homemade anodic bonding setup was used. It consisted of a digital hotplate, ceramic insulator, aluminum electrode, brass electrode, and a high voltage power supply. A schematic of the setup is shown in figure 1.8.

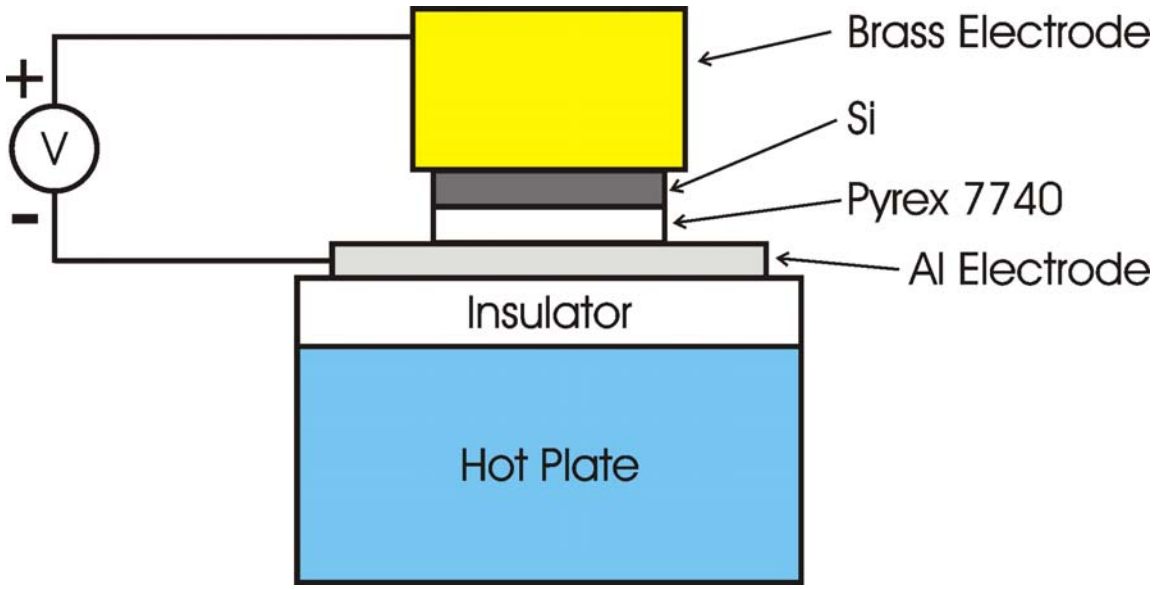

Figure 1.8. Schematic of the anodic bonding setup.

CHAPTER II

EXPERIMENTAL

2.1 Array Chip Fabrication

The array chip used in chapter IV was fabricated using standard photolithographic techniques. The process begins with the cleaning of 1 in. square microscope cover slips by boiling them in a 10% 7X detergent solution for 20 min. The slides are removed from the solution while still warm and rinsed with three alternating cycles of ethanol and purified water (18 MΩ/cm^2, NANOpure Ultrapure Water System, Barnstead, Dubuque, IA). The slides are then dried under a stream of nitrogen gas and annealed at 450°C for 5 hrs. Next, the cover slips were coated with 1000 Å of chrome by metal evaporation (BOC Edwards Auto 306 Metal Evaporation Chamber, Wilmington, MA). Approximately 6 μm of photoresist is spun onto the chrome coated slides using a homemade resist spinner consisting of an AC motor and a variable transformer. The freshly spun on photoresist was baked at 90°C for 45 min in a toaster oven (Black & Decker). A photomask for the array chip was designed in CorelDraw and reduced onto 35 mm film as a negative.[3] The negative was affixed to a microscope slide with double sided tape to produce the finished photomask. The photoresist is then exposed to UV radiation from a Quintel Q400MA mask aligner (San Jose, CA). UV illumination through the photomask destroys the photoresist, which, after developing,

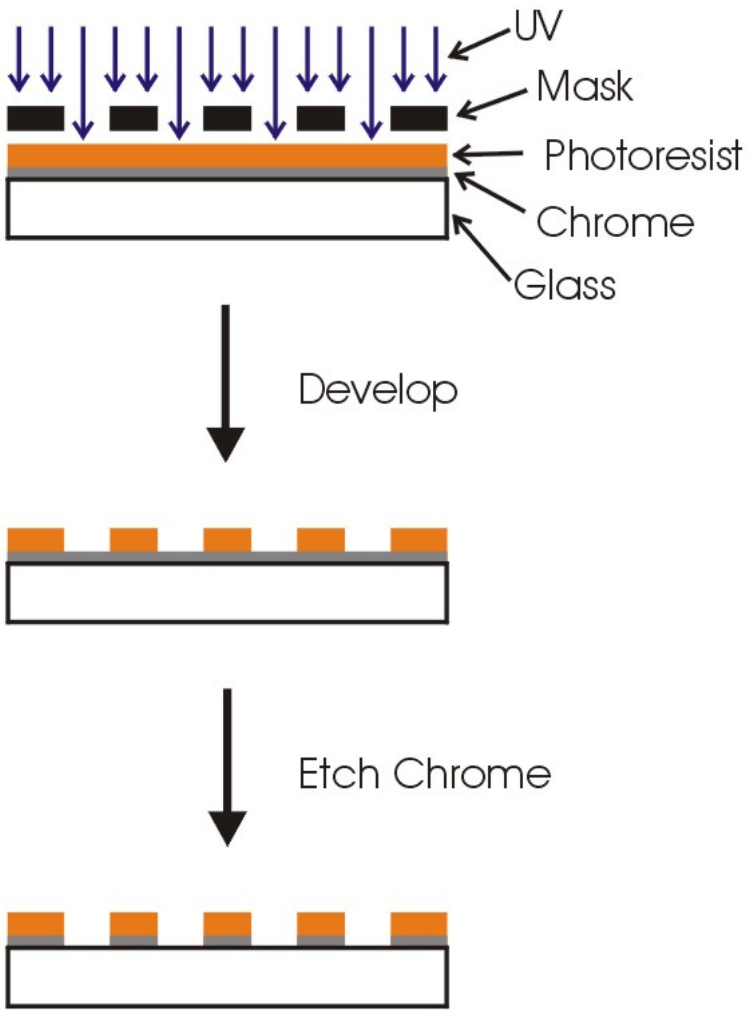

Figure 2.1. Array chip fabrication process.

leaves a 10 x 10 array of 0.6 mm square boxes separated by 0.4 mm hydrophobic photoresist walls. The exposed chrome is then removed using commercial chrome etchant, yielding an array of hydrophilic glass plates with hydrophobic photoresist walls. A schematic of the process is shown in figure 2.1.

2.2. Spatial Addressing

Microcapillary tips used to address vesicle solutions onto the array chips were prepared according to Yang et al.[14] 1.5 mm O.D. capillary tubes (World Precision Instruments, Sarasota, FL) were pulled in a micropipette puller (Sutter P-97, Sutter Instrument, Novato, CA) to an outer diameter of less than 10 μm using the following settings, temperature = 365° C, velocity = 125 microns/sec, and time = 200 sec. These tips were then treated with 1,1,1,3,3,3-hexamethyldisilazane vapor in a 75° C oven to render their surface hydrophobic. This allows for easy transfer of vesicle solution from the tip to the glass surface. By attaching the pulled capillary to a 100 μL micropipette, the dispensing of droplets to the surface of the array chip can be controlled. To perform the addressing, an array chip is placed on a cold plate as described elsewhere[14] and the temperature of the chip is adjusted to just above the dew point in order to minimize evaporation of the addressed solutions. A sample of 35 μL is drawn into the tip using the micropipette and pressure on the solution is adjusted until the desired size droplet is dispensed from the tip. The droplet size optimization is carried out by delivering

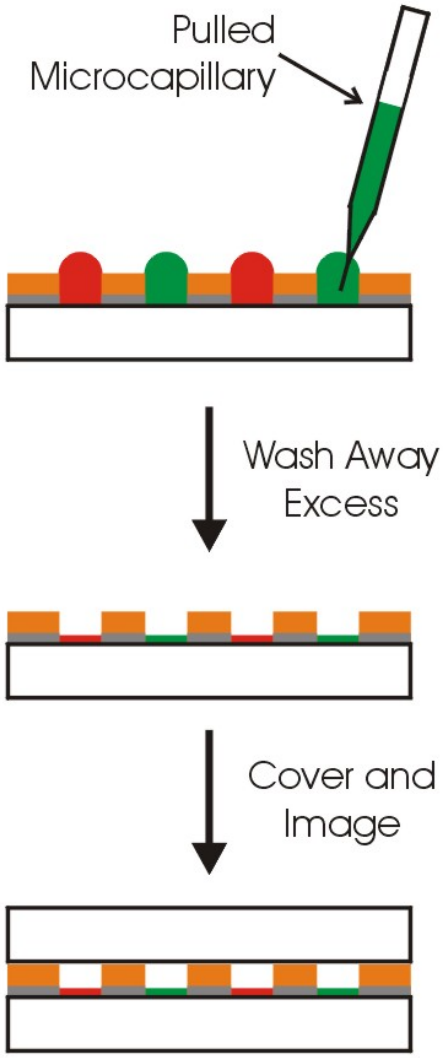

Figure 2.2. Addressing of the array chip. A pulled capillary is used to address individual hydrophilic glass plates with red and green vesicles.

droplets to a secondary array chip. The solution is then delivered to the desired box on the array chip and the tip is cleaned before the next solution is addressed. An illustration of the addressing process is shown in figure 2.2. Once the array chip is fully addressed, the chip is submerged in purified water to remove excess vesicles. At this stage, if it is desired, the array chip can be incubated with an analyte protein solution using a polydimethylsiloxane well and a humidity chamber. The humidity chamber is constructed by inverting a small crystallization dish inside of a larger crystallization dish. The array chip and PDMS incubation well are placed on top of the smaller crystallization dish, a small amount of water is added to the larger dish and the system is covered (figure 2.3). After incubation, the solution in the PDMS well is carefully exchanged with PBS buffer and the chip and well are submerged in PBS buffer. The well is removed from the array chip and the chip is then covered with a microscope cover slip to keep the SLB array hydrated during imaging.

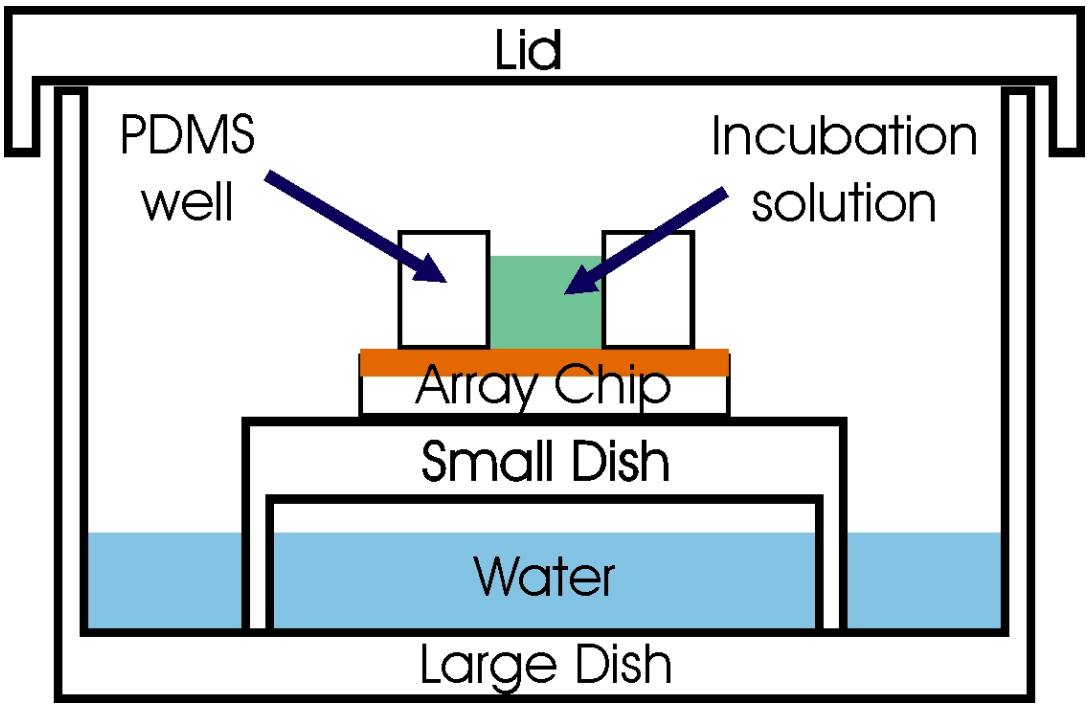

Figure 2.3. A schematic of a homemade humidity chamber. A small crystallization dish is inverted inside a large crystallization dish. Samples placed inside along with water allow for extended incubations with minimal evaporation.

CHAPTER III

DIRECT WRITING OF METAL NANOPARTICLE FILMS INSIDE SEALED MICROFLUIDIC CHANNELS

3.1. Synopsis

In this chapter we demonstrate the ability to pattern Ag nanoparticle films of arbitrary geometry inside sealed PDMS/TiO2/glass microfluidic devices. The technique can be employed with aqueous solutions at room temperature under mild conditions. A 6 nm TiO_2 film is first deposited onto a planar Pyrex or silica substrate, which is subsequently bonded to a PDMS mold. UV light is then exposed through the device to reduce Ag^+ from an aqueous solution to create a monolayer thick film of Ag nanoparticles. We demonstrate that this on-chip deposition method can be exploited in a parallel fashion to synthesize nanoparticles of varying size by independently controlling the solution conditions in each microchannel in which the film is formed. The film morphology was checked by atomic force microscopy and the results showed that the size of the nanoparticles was sensitive to solution pH. Additionally, we illustrate the ability to biofunctionalize these films with ligands for protein capture. The results indicated that this could be done with good discrimination between specific locations and background. The technique appears to be quite general and films of Pd, Cu, and Au could also be patterned.

3.2. Introduction

Chemically patterned surfaces within the confines of microfluidic channels enhance the flexibility and utility of lab-on-a-chip platforms.[3,165-167] For complex systems, significant attention has been focused on aligning pre-patterned substrates with separately molded microchannels.[168-171] However, devising simple methods for controlling the surface chemistry inside microfluidic channels after device assembly could greatly enhance rapid prototyping capabilities. In fact, precise spatial control over the molecules presented on the channel walls avoids the need to bring pre-patterned substrates into registry and allows materials to be utilized that cannot easily withstand harsh bonding procedures. Such issues can be critical in the design of microfluidic based sensors, diagnostic devices, and microreactors. Until now, patterning inside sealed microfluidic devices has been quite challenging. This is especially true if one is interested in deposition methods involving aqueous solutions and mild conditions. There have been some strategies developed for organic and biological materials,[144] but procedures for addressing metals are particularly limited.[172]

Typically, metal patterning of substrates is carried out via top down methods beginning with the evaporation or sputtering of metal onto a substrate. This step is followed by either spin coating and lithographic patterning of photoresist or microcontact printing of thiol polymer multilayers.[173] Both procedures provide a protective masking layer during chemical etching of the unwanted regions of the deposited metal. Such procedures work extremely well for patterning planar substrates, but would be extremely challenging to carry out inside enclosed polydimethylsiloxane

and glass microfluidic systems because of the impracticality of sputtering, stamping, or spin coating materials inside enclosed architectures. Another approach has been to photoreduce metals from polymer solutions and films onto planar substrates.[174,175] Unfortunately, such methods would be cumbersome to employ in microchannel networks as the macromolecular catalysts for metal reduction would be hard to remove after the metal is deposited.

Currently, the most practical strategy available for patterning metals inside sealed microchannels involves the use of multiphase laminar flow.[172] Similar techniques have also been exploited for the patterning of polymers,[176] inorganic crystals, proteins, and cells.[177] These methods, however, produce architectures which are limited by the flow profiles generated within specific channel geometries, and often must be formed downstream from a channel junction. We therefore aimed to devise a simple procedure that would allow metal films to be patterned inside sealed microfluidic systems from an aqueous solution under mild conditions with almost any design.

TiO_2 is a well known photocatalyst for water and air purification.[178] UV illumination produces electrons and holes that can be used to oxidize and reduce a wide range of organic and inorganic species on its surface, including metal ions from aqueous solutions. In particular, photocatalytic deposition of Ag into a sol-gel derived TiO_2 matrix and onto TiO_2 particles has been shown to occur from Ag^+ in aqueous solution.[179-183] Adsorbed Ag^+ ions are reduced by the photogenerated electrons and water undergoes oxidative decomposition by the holes.[184] This process typically generates metal nanoparticles, where the particles vary in size and shape depending upon

the exact conditions employed.[185] Such methods have been extended to patterning metals onto TiO_2 nanoparticles at interfaces[186] and should even be useful for patterning inside microfluidic channels if a thin TiO_2 coating on a planar support were used instead of the nanoparticles. Indeed, we reasoned that this would be possible as long as the distance the electron/hole pair diffused from the initial site of excitation was fairly restricted. The utility of the technique lies in the fact that the surface of the microchannel itself would now be the catalyst for metal deposition. Such a technique is compatible with aqueous solutions and ambient conditions, which is ideal for microchannel surface modification.

Our strategy for patterning Ag nanoparticle films involves the reduction of Ag^+ from an aqueous $AgNO_3$ solution by selectively illuminating the desired areas of the microchannel with UV radiation through a photomask. After a metal film has been deposited, its surface can be further tailored by employing thiol chemistry. In fact, we found that the serial introduction of metal patterns at specific locations, followed by surface derivatization easily led to the presentation of spatially addressed biosensor architectures (figure 3.1). Moreover, several different metals including Pd could be patterned in addition to silver.

3.3. Methods and Materials

Materials

Polished Pyrex 7740 wafers (25.4 mm^2, 0.5 mm thick) were supplied by Precision Glass and Optics (Santa Ana, CA). Fused silica cover slips (25 mm^2, 0.17 mm thick) were purchased from Structure Probe, Inc. (West Chester, PA). Biotin PEG disulfide (figure 3.2.A), and PEG propionate disulfide (figure 3.2.B) were obtained from BioVectra Inc (Prince Edward Island, Canada). N-(2,4-dinitrophenyl)cadaverine hydrochloride (DNP-cadaverine) was acquired from Axxora (San Diego, CA). Streptavidin Alexa Fluor 594 conjugate (Strep-A594), anti-dinitrophenyl-KLH, rabbit IgG fraction, and Alexa Fluor 488 conjugate (anti-DNP-A488) were supplied by Invitrogen (Eugene, OR). Polydimethylsiloxane (Dow Corning Sylgard Silicone Elastomer-184) was obtained from Krayden, Inc (El Paso, TX). Silver nitrate, palladium chloride, *N*-ethyl-*N'*-(3-dimethylaminopropyl)carbodiimide hydrochloride (EDC), sodium phosphate, 4-(2-hydroxyethyl)piperazine-1-ethanesulfonic acid (HEPES buffer salt), and sodium chloride were purchased from Sigma-Aldrich (Saint Louis, MO). These materials were used as provided.

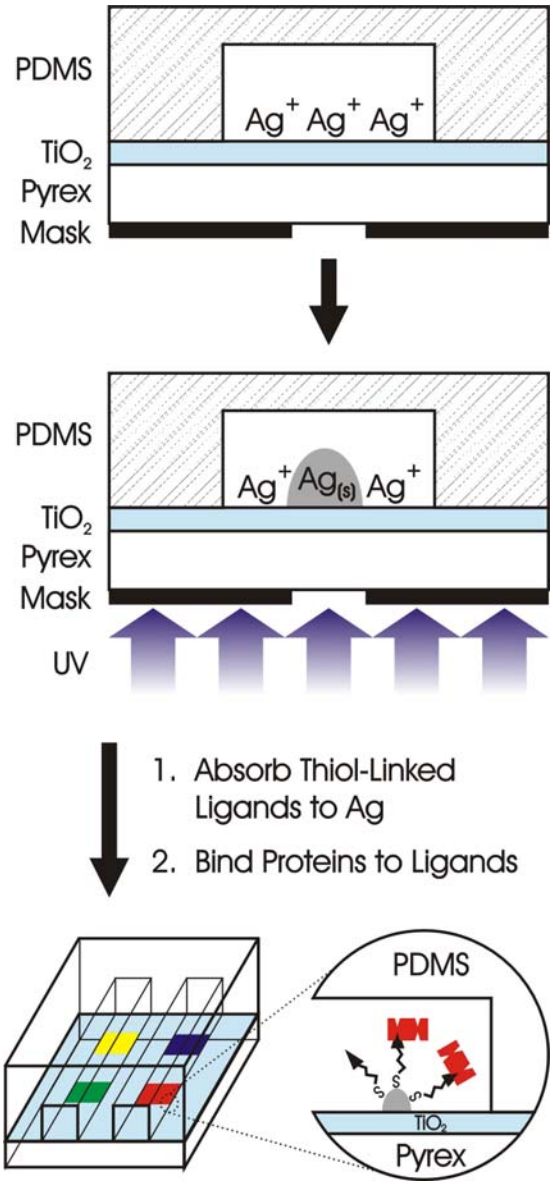

Figure 3.1. Schematic diagram for the deposition of a silver nanoparticle film. UV radiation is passed through a photomask onto the backside of a TiO_2 thin film. Ag^+ ions adsorbed at the interface are selectively reduced by photoelectrons, which grow into nanoparticle films. This process can be used in combination with thiol chemistry inside sealed microfluidic channels to address surface chemistries in almost any desired location or pattern.

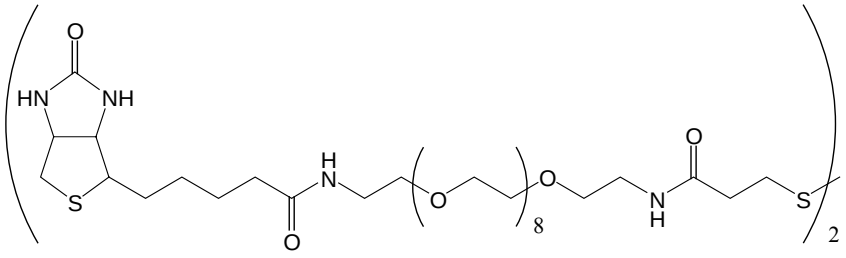

(A) Biotin PEG disulfide.

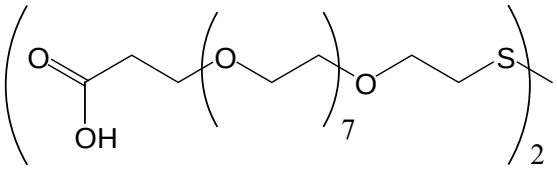

(B) PEG propionate disulfide.

Figure 3.2. Structures of (A) Biotin PEG disulfide and (B) PEG propionate disulfide.

TiO_2 Film Preparation

Smooth films of TiO_2 were prepared using our previously established room temperature and pressure chemical vapor deposition protocol.[110] The film is grown via hydrolysis of titanium (IV) isopropoxide by OH groups on the substrate surface aided small amounts of water vapor.[187,188] This process occurs inside the reaction chamber producing isopropanol and TiO_2. Briefly, Pyrex 7740 wafers or silica cover slips were cleaned in piranha solution (1:3 ratio of 30% H_2O_2 and H_2SO_4, *note: piranha is a vigorous oxidant and should only be used with extreme caution*) for 45 min., rinsed extensively with purified water (18.2 MΩ/cm^2, NANOpure Ultrapure Water System, Barnstead, Dubuque, IA), dried with nitrogen, and baked at 500°C for 5 hrs. The wafers were then soaked in concentrated H_2SO_4 for 6 hrs, rinsed extensively with more purified water, rinsed with methanol, dried with nitrogen, and exposed to titanium (IV) isopropoxide vapor at room temperature for 2 hrs. The surface reaction was stopped by rinsing with purified water and reagent grade acetone. Finally, the slides were baked again at 500°C for 5 hrs to facilitate calcination of the film. The thickness of the titania layer was measured to be 6 nm by ellipsometry (model L2W26D; Gaertner Scientific, Skokie, IL), using a 632 nm laser at 80º and assuming the index of refraction of the film was 2.46.[189,190]

Microfluidic Device Fabrication

Polydimethylsiloxane (PDMS) microfluidic devices were fabricated using previously published soft lithography techniques.[3] The microfluidic devices consisted of five 300 μm wide by 8 μm deep channels. The PDMS and TiO_2/glass surfaces were treated with an oxygen plasma for 10-15 sec and immediately brought into contact with each other to create a bond. This formed channels with PDMS walls and a TiO_2 floor.

Synthesis of *N*-(2,4-Dinitrophenyl) PEG Disulfide

In 100 mL of HEPES buffer (10 mM HEPES, pH 7.4), 1 equivalent of PEG propionate disulfide (2 mM) was reacted with 2 equivalents of DNP-cadaverine in the presence of 3 equivalents of EDC. The EDC coupling reaction was allowed to proceed for 24 hrs at room temperature in the dark under constant agitation. The formation of *N*-(2,4-dinitrophenyl) PEG disulfide (DNP-PEG-disulfide) was confirmed by matrix assisted laser desorption ionization (MALDI) mass spectrometry..The structure of DNP-PEG-disulfide is shown in figure 3.3.

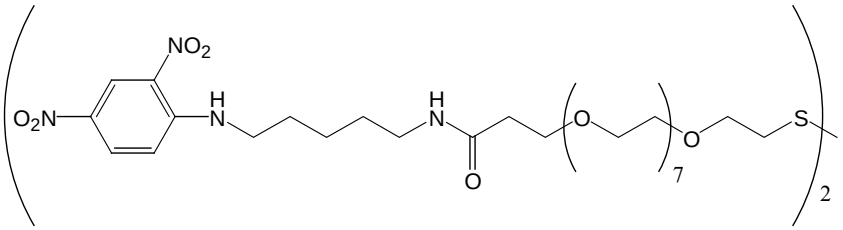

Figure 3.3. Structure of DNP-PEG-disulfide.

Direct Writing of Silver Films

Thin silica cover slips (0.17 mm) coated with TiO_2 films were used for higher resolution Ag patterns and thicker (0. 5 mm) Pyrex supports were used in all other cases. UV patterning of Ag films was performed with a mask aligner (Quintel Q400MA, San Jose, CA) through a high resolution test mask (Edmund Industry Optics, Barrington, NJ). The patterned Ag films were imaged using brightfield illumination on a Nikon Eclipse 80i fluorescence microscope with a Princeton Instruments 1024B MicroMax CCD camera (Trenton, NJ). The same instrument was used for fluorescence imaging. Individual false color images of the fluorescence from the bound strep-A594 and anti-DNP-A488 in the sealed microchannels were combined in Adobe Photoshop 5.0. For Ag patterning experiments performed as a function of pH, the pH value of the silver solutions was adjusted with appropriate amounts of HNO_3 or NaOH. AFM imaging was performed with a Nanoscope IIIa (Digital Instruments, Santa Barbara, CA) equipped with a J-type scanner and silicon cantilever tips (Mikro Masch, Wilsonville, OR).

3.4. RESULTS

Direct Writing of Silver Films

In a first set of experiments, a solution of 0.1 M $AgNO_3$ at pH 5.0 was injected into a series of five parallel microfluidic channels. The channels consisted of PDMS walls and a TiO_2 floor. UV light (11 mW/cm^2 near 365 nm) was used to selectively illuminate different regions of the TiO_2 surface through a chrome test mask for 20 min. This resulted in the direct writing of silver by photocatalytic reduction inside the

microchannels as could be verified by brightfield imaging of the device (Figure 3.4.A). The chemical composition of the film was verified by XPS (Kratos Axis Ultra Imaging X-ray photoelectron spectrometer, Manchester, U.K). As can be seen, the film could be patterned with nearly any geometry desired and the feature resolution was ~10 μm.

Next, we wished to verify that Ag nanoparticle films could be patterned with at least micron-scale resolution. This required the use of a thinner support beneath the TiO_2 coated surface as UV light for patterning is introduced through the back of the substrate (figure 3.1). In order to minimize feature distortion due to imperfect illumination conditions, a 0.17 mm silica slide was used as the support. This thinner support was chosen because light from a less-than-perfectly collimated source will lead to increasingly poorer image resolution the further the mask is offset from the TiO_2 film. The reason for employing silica rather than Pyrex stemmed from the fact that thinner silica substrates were more readily available from commercial sources. The results showed that patterns could easily be made with resolution down to a few microns (Figure 3.4.B). For example, the red arrow points to a series of 6 μm wide lines separated from one another by 6 μm spaces. The ultimate resolution of the mass aligner employed is about 2 μm. It should be noted that control experiments were performed with thicker silica substrates. The results demonstrated that patterning Ag films on TiO_2/silica behaved similarly to TiO_2/Pyrex under conditions of identical substrate thickness.

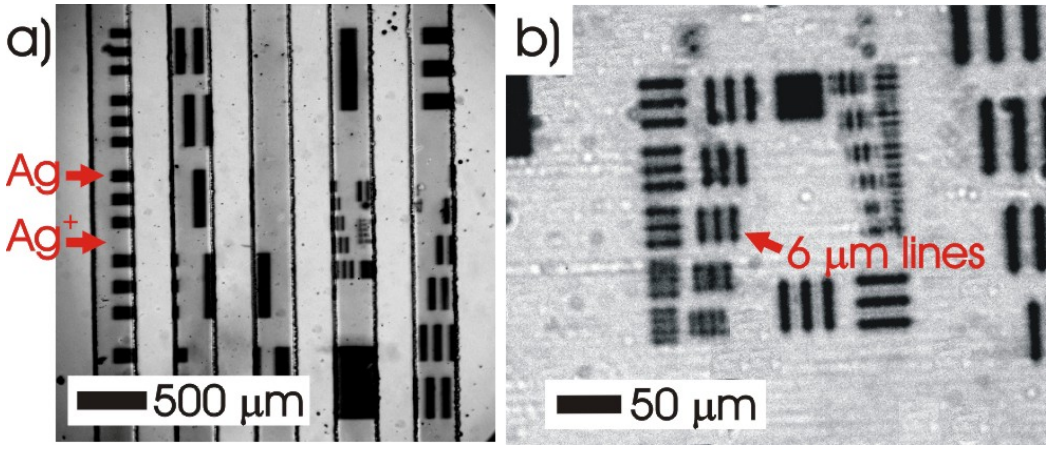

Figure 3.4. (a) Brightfield image, 4X, of silver nanoparticles patterned inside sealed microfluidic channels by lithographic photocatalytic deposition. Each channel has a width of 300 µm. (b) Brightfield image under a 40X objective pointing out 6 µm wide lines.

Controlling Film Morphology at the Nanoscale

The ability to deposit Ag films inside microfluidic channels opens the door to on-chip studies of film morphology as a function of deposition conditions. To demonstrate this, experiments were performed as a function of the pH of the $AgNO_3$ solution. It is known that the pH of Ag^+ solutions affects the rate of silver deposition as well as the initial amount of Ag^+ adsorbed onto a TiO_2 surface.[191] This is caused in large part by the modulation in surface charge of the TiO_2 substrate as the pH is changed. We therefore reasoned that particle size might vary as the deposition pH is changed over the planar substrate. The deposition conditions were otherwise similar to those used in figure 3.4. However, to enable investigation of nanoparticle size by AFM, the $AgNO_3$ solutions were injected into PDMS microchannels that were only pressed against the TiO_2 surface rather than plasma bonded with it. This allowed the PDMS mold to be pealed away from the substrate just prior to investigation by AFM. The substrate was rinsed with purified water and blown dry with N_2 gas before imaging in air. Deposition was undertaken at pH 2, 3, 5, and 6 and AFM images of the surface under the various conditions are shown in figure 3.5.

The AFM results show that the mean particle size was 65 nm at pH 2 and image analysis revealed that the 1σ particle size distribution was 24 nm (figure 3.5.A). Under these conditions the surface is positively charged, hence, limiting the rate of Ag^+ adsorption. This should lead to sparse nucleation sites and larger particles. As the pH is raised, the coverage becomes higher for fixed deposition time (20 min) and the mean

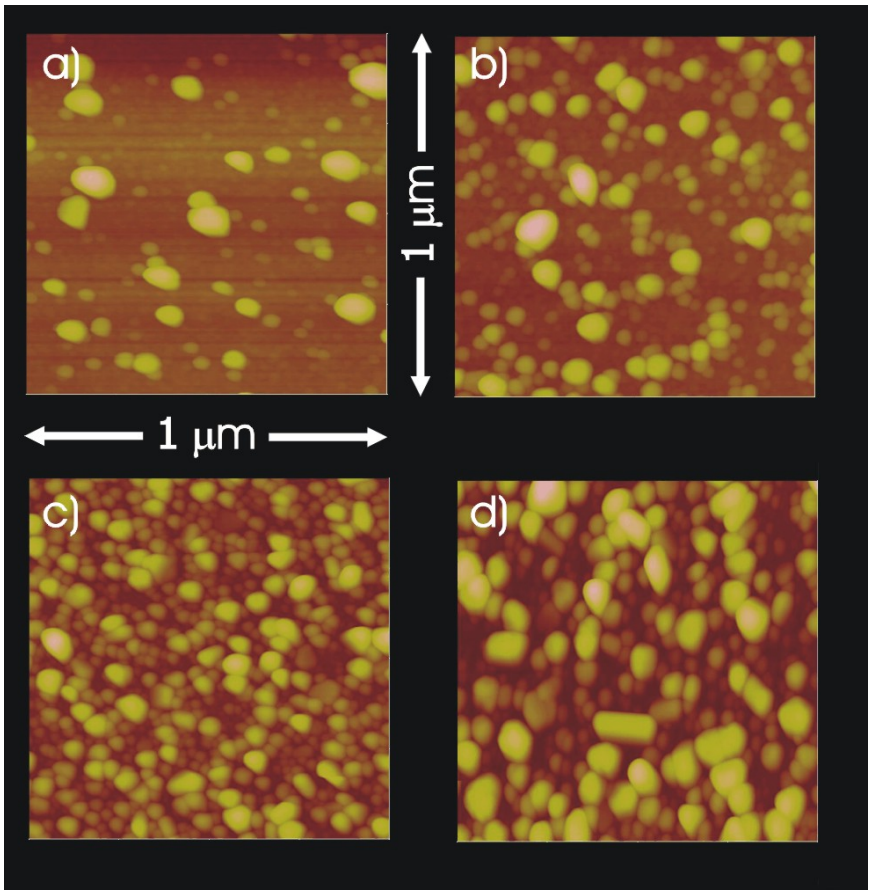

Figure 3.5. Tapping mode AFM images of Ag nanoparticle films deposited at (a) pH 2, (b) pH 3, (c) pH 5, and (d) pH 6.

nanoparticle size begins to decrease (figure 3.5.B & 3.5.C). In these cases the particle sizes were 62 nm with 1σ = 16 nm at pH 3 and 51 nm with 1σ = 16 nm at pH 5. Above the isoelectric point of the TiO_2 film (pI ≅ 5.5), the size again increases as does the relative surface coverage (mean particle size of 75 nm with 1σ = 26 nm at pH 6). These results clearly demonstrate that at least limited control over nanoparticle size and coverage can be obtained through modulation of the bulk solution pH.

Sensor Chip

In order to demonstrate the versatility of this technique for sensor design and biofunctionalization within sealed microchannels, a simple two color fluorescence assay was developed wherein two separate ligands were patterned at different locations within a linear array of microfluidic channels. First, a strip of silver was patterned across 3 sealed microfluidic channels using the procedures described above. The channels were rinsed with purified water, filled with a solution of 2 mg/mL biotin PEG disulfide and 10 mg/mL PEG propionate disulfide in HEPES buffer (10mM HEPES, pH 7.4) and allowed to incubate overnight. The channels were then rinsed with purified water to leave behind films with biotin termination. After this, the channels were again filled with a 0.1 M $AgNO_3$ solution and another strip of silver was patterned downstream from the first one. The channels were rinsed and incubated with a solution containing DNP-PEG disulfide and 10 mg/mL PEG propionate disulfide in HEPES buffer for 30 min. Finally, the channels were rinsed and incubated with a 1 mg/mL solution of bovine serum albumin in

PBS buffer (10mM PBS, pH 7.2, I = 150 mM with NaCl) to block nonspecific adsorption of the analyte proteins.

After rinsing all three channels with buffer, various protein solutions were injected into each channel: (1) 0.1 mg/mL strep-A594 in PBS buffer, (2) a mixture of 0.1 mg/mL strep-A594 and 0.1 mg/mL of anti-DNP-A488 in PBS buffer, and (3) 0.1 mg/mL anti-DNP-A488 in PBS buffer. After 20 min of incubation, the channels were rinsed for a final time with PBS buffer and fluorescence images were obtained with both a green and red filter set. The combined false color image is shown in figure 3.6. The image clearly demonstrates that the streptavidin (labeled red) binds almost exclusively to regions within the channel where the Ag nanoparticle film has been functionalized with biotin, while the anti-DNP antibody (labeled green) binds overwhelmingly at regions within the channel where the DNP was presented.

The data in channel 2 demonstrate the binding of both proteins from the same solution to different locations with good selectivity, illustrating the possible multiplexing and combinatorial potential for this technique. Figure 3.7 shows the normalized fluorescence intensity of the specifically bound proteins (blue) compared to the background signal from non-specific interactions in the middle of the channel (yellow) as well as the non-specific interactions at the sensor pad presenting the opposite ligand (brown). In all cases the specific binding of analyte proteins was between one and two orders of magnitude greater than non-specific absorption.

These simple experiments illustrate the ability of this method to pattern unique chemistries such as small molecules and proteins inside sealed microfluidic channels at

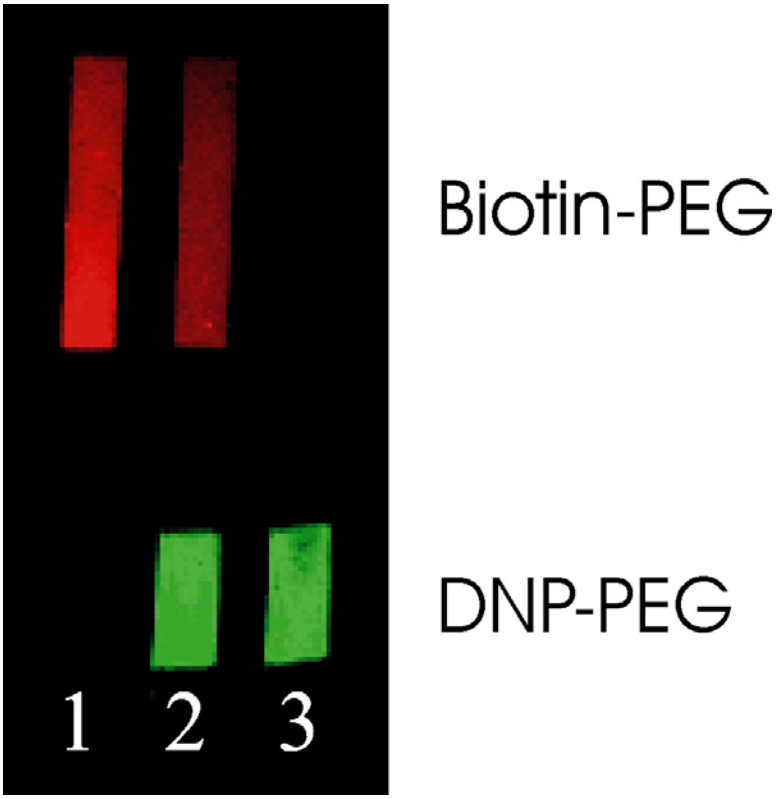

Figure 3.6. Fluorescence micrograph of fluorescently labeled proteins binding to derivatized silver nanoparticles. Channel 1 was injected only with streptavidin (red) and shows evidence of it binding almost exclusively to the biotin derivatized nanoparticles, while the rest of the channel remains dark. Channel 3 was injected with anti-DNP (green), which is observed to bind only to the DNP derivatized nanoparticles. Channel 2 was injected with both proteins and, hence, both binding events occurred.

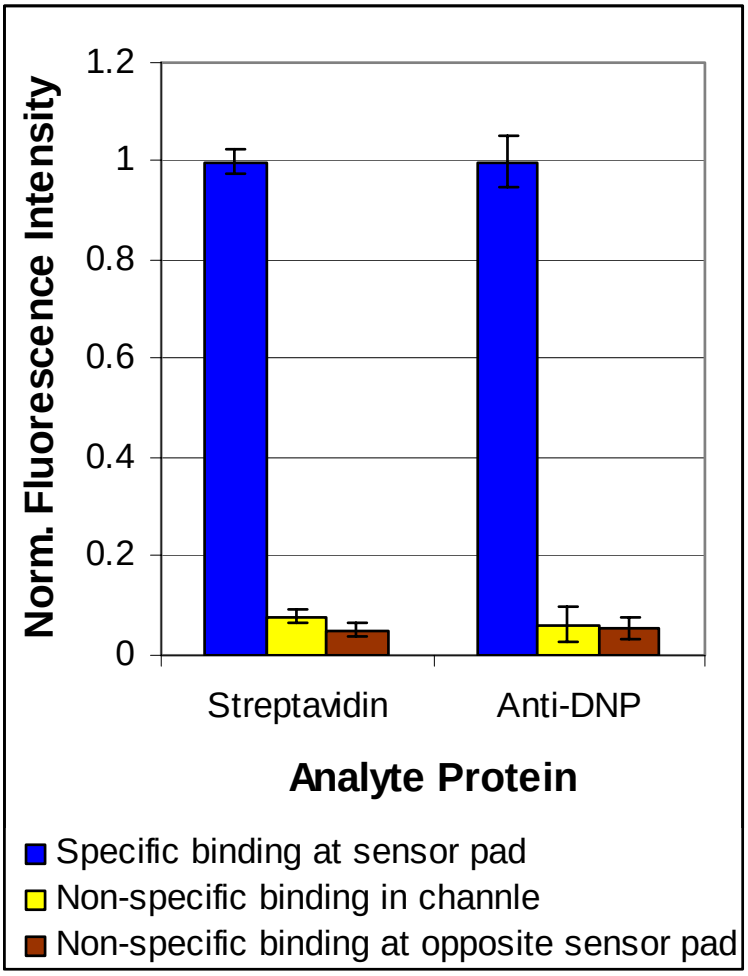

Figure 3.7. Bar graph of the normalized fluorescence intensity of analyte proteins binding specifically to their respective sensor pads (blue), analyte non-specifically binding in the channel (yellow) and non-specific adsorption at the opposite sensor pad (brown).

specific addresses. In this case our post-assembly patterning method is useful for avoiding the exposure of patterned organic ligands to the harsh bonding conditions (i.e. oxygen plasma treatment) of PDMS to the TiO_2 surface.

This simple experiment illustrates the ability of this method to pattern unique chemistries such as small molecules and proteins inside sealed microfluidic channels at specific addresses. In this case our post-assembly patterning method is useful for avoiding the exposure of patterned organic ligands to the harsh bonding conditions (i.e. oxygen plasma treatment) of PDMS to the TiO_2 surface.

Patterning Other Metals

TiO_2 nanoparticles can be used for the reduction of a variety of metals.[183] Therefore, the technique developed above for patterning silver should be generally applicable. Figure 6 shows the direct write patterning of Pd (Figure 3.8). In this case, Pd was deposited from a solution of 0.01 M $PdCl_2$ in 0.3 M acetic acid with a 20 min UV exposure onto a TiO_2 surface supported by a 0.5 mm thick Pyrex substrate. As with silver, the method appears to be highly robust and easily performed inside sealed microfluidic channels. We have also successfully repeated this work with Cu and Au, although the nanoparticle sizes were somewhat larger.

3.5. Discussion

The writing of metal nanoparticle films could be exploited for a variety of applications inside sealed microfluidic devices and the technique is probably capable of near diffraction limited resolution. In the work presented herein, the resolution was somewhat limited by backside illumination. In other words, the backside contact mask procedure employed, in which light must transverse the thickness of the substrate, was the limiting factor rather than any inherent physical limit due to electron diffusion within the TiO_2 film. Using literature values for the electron diffusion coefficient in TiO_2, $D = 2.2 \times 10^{-5}$ cm^2/s,[192] as well as the electron-hole recombination lifetime, $\tau = 50$ ns,[193] it can be estimated in a simple two-dimensional random walk model, $L = (4Dt)^{1/2}$, that photogenerated electrons should diffuse only about a length, L, of 20 nm before recombining under the conditions we employ. The exact recombination lifetime depends on the intensity of the light used.[194] This calculation also assumes that the films are free of defects and, therefore, the actual travel distance may be even shorter for real films. Therefore, in the case of patterning with 365 nm light, the ultimate resolution should be close to 200 nm if high quality projection optics were to be employed in the patterning procedure.

Using the methods described herein, it should be possible to rapidly screen the effects of Ag^+ concentration, temperature, and surfactant additives on metal nanoparticle size and geometry. This would be especially useful for particles deposited in pH, composition, and/or temperature gradients.[191,195] Furthermore, it should be possible to employ this lab-on-a-chip format for patterning not

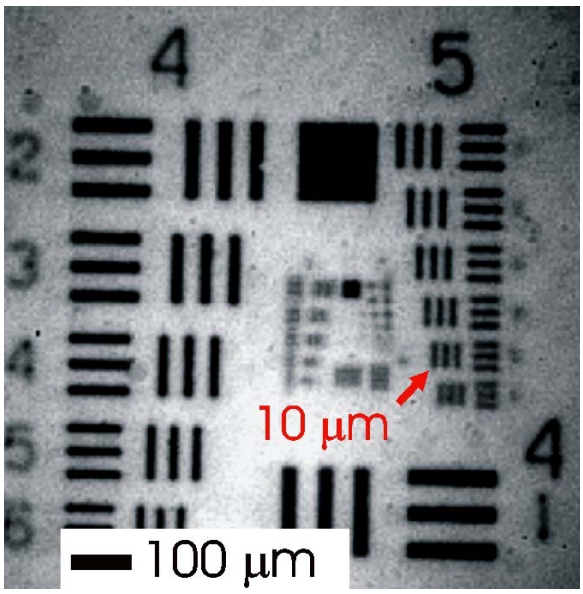

Figure 3.8. Brightfield image, 10X, pattern of Pd deposited onto TiO_2.

just individual metals but also for alloys, core shell structures,[196,197] and even gradient arrays of various metals. The use of microfluidics in this case offers the ability to rapidly optimize such deposition processes in a combinatorial manor. It could also allow for these materials to be exploited for high throughput screening of catalytic properties, sensor development, and microreactor design.

Functionalizing the nanoparticle films inside of microfluidic channels may offer new opportunities for biosensors or screening assays. The ability to address individual ligands atop nanoparticle films inside microfluidic devices could be combined with such technologies as transmission surface plasmon resonance spectroscopy[198-201] or surfaced enhanced fluorescence.[202-204] This could allow for the development of powerful lab-on-a-chip devices with label free detection or fluorescence detection with enhanced sensitivity.

Immobilizing patches of oriented enzymes inside microfluidic devices for enzymatic microreactors is another potential application of this technique. By binding enzymes linked to antibodies or streptavidin one could spatially address arrays of enzymes inside microfluidic devices for the development of complex enzymatic microreactors. Such reactors could perform a series of chemical modifications to a substrate within a single channel. This process might even be multiplexed across several channels utilizing a variety of enzymes for combinatorial synthesis.

CHAPTER IV

AN EPIFLUORESCENCE/TOTAL INTERNAL REFLECTION MACROSCOPE FOR THE IMAGING OF LARGE ARRAYS OF SOLID SUPPORTED LIPID BILAYERS

4.1. Synopsis

Herein we present the design and construction of an epifluorescence/total internal reflection (EF/TIRF) macroscope for large field of view and high numerical aperture imaging of spatially addressed arrays of solid supported phospholipid bilayers. This instrument allows dozens of individually addressed bilayers to be monitored simultaneously. To demonstrate the capabilities of the EF/TIRF macroscope, three experiments have been performed: (i) the fabrication of an array of bilayers with all phospholipid membranes individually addressed at each location, (ii) a multiple protein recognition assay designed to show the effects of ligand density on the total amount of aqueous protein which can be bound at equilibrium, and (iii) a fluorescence resonance energy transfer assay between two different dyes confined within the same solid supported lipid bilayer as a function of the concentration of each dye. These results clearly open the door to using individually addressed bilayers for a variety of supported membrane-aqueous phase analyte interactions in a high throughput fashion. The key to the successful implementation of the assays was making the field of view wide enough

so that individual bilayers could be addressed via a convenient droplet transfer mechanism.

4.2. Introduction

Fluorescence microscopy has proven to be an invaluable tool for the investigation of supported lipid bilayers inside microfluidic devices[17,195,205-207] and on array-based platforms.[13,14,208-213] When combined with total internal reflection (TIR) illumination, this technique becomes even more powerful, allowing the user to investigate surface specific binding events that occur between surface-associated membrane bound ligands and aqueous proteins containing complementary receptor sites.[3,207,214] Imaging arrays of bilayers with fluorescence microscopy has been possible by shrinking the membrane patches to the micron scale. This technique has been especially valuable for making one-shot equilibrium dissociation constant measurements in which the contents of each bilayer is identical, but the aqueous solutions above them contained various protein concentrations.[3]

While fluorescence microscopy has the advantage of one shot imaging, it is limited in its field of view. In order to employ a platform with more individually addressable membrane patches, one either needs to shrink the size of the patch or expand the field of view. Excellent methods are now available for creating micron-scale patterning for lipid bilayers. [13,14,17,20,208,209,212,213,215-217] So long as each bilayer in the array is chemically equivalent to the others, patterning can be scaled down to the 1 micron level or even below. On the other hand, there are a limited number of methods available for making arrays with variable contents at each address in micron scale

patterns. One method is to employ the laminar flow of vesicle solutions side by side inside a microfluidic device.[17] This creates a gradient of bilayer chemistries that can be confined by a patterned surface. This method is, however, limited in the number of unique chemical constituents that can be patterned and also spatial control over the patterned membrane arrays is somewhat difficult. Another method for patterning unique lipid membrane chemistries relies on the use of PDMS stamping and backfilling.[212] Again this method can fabricate arrays with a few unique chemistries, but spatial alignment limits this number for practical rapid prototyping. Several light directed methods have also been developed for the patterning of lipid bilayers.[208,215,216] However, such techniques have not been proven for patterning of more then two component systems and addressing needs to be performed in a serial fashion.

Fully controlled spatial address of lipid bilayers with unique chemistries at every location has been achieved by transferring picoliter and nanoliter-sized droplets of vesicle solutions to a hydrophilic interface patterned with hydrophobic barriers (microcapillary injection method);[14] however, the array size has been typically limited to 3 x 3 or 4 x 4 because of the need to pattern all the contents within a field of view that is compatible with imaging by fluorescence microscopy. Smaller box sizes become impractical below about 50 μm because of the need to fabricate quill pen tips that would transfer the aqueous solution. In fact, the method already becomes tedious to employ for large arrays of boxes of approximately 250 μm on each side. On the other hand, larger fields of view could be achieved by building an appropriate epifluorescence/total internal reflection macroscope. This would allow dozens if not hundreds of unique bilayers chemistries to be easily patterned on a larger size scale and analyzed in a single

experiment. One problem in using lower magnification objectives for large field of view imaging is that the numerical aperture (N.A.), or light gathering capability of a fluorescence imaging system, typically decreases with decreasing magnification. In order for the magnification to be decreased, the working distance (distance between the objective and the sample) must be increased. By increasing the working distance and maintaining a fixed objective diameter, one unfortunately also reduces the cone angle of light, which can be collected by the system from a given point on the sample. Low N.A. imaging therefore requires longer exposure times, which decreases the signal to noise ratio and increases the amount of photobleaching in the sample. An easy way around this problem is to build a system with both long working distances and large diameter objectives. The desire for high N.A. fluorescence imaging of large fields of view has been the driving force for the construction of an EF/TIRF macroscope.

Epifluorescence macroscopes employing 1x objectives have already been developed for imaging animal tissues[218-220] The basic design uses a tandem-lens imaging system much like that in X-ray video radiography and up-close photography.[221] These instruments have seen limited employment for imaging protein arrays on chip. To the best of our knowledge, however, a total internal fluorescence reflection macroscope has not previously been developed.

Herein we demonstrate the ability to fabricate dozens of uniquely addressed phospholipid bilayers and image them in a single shot with an epifluoresence/total internal reflection fluorescence macroscope. Further experiments show fluorescence quenching as a function of probe density as well as ligand-receptor binding assays. These experiments clearly demonstrate for the first time the ability to array large

numbers of bilayers with unique chemistries at each address and employ them in model membrane studies.

4.3. Methods

Macroscope Design

We have designed a unique low magnification, high N.A. fluorescence imaging system compatible with monitoring supported phospholipid bilayers. The system is equipped with multiple filter sets that can be rapidly interchanged (just like in standard fluorescence microscopes) as well as a separate port for total internal reflection fluorescence microscopy experiments. This represents the first design of a fluorescence macroscope with exchangeable filter sets. This is made possible by mounting the filters and dichroic mirrors on mounts which ride on a system of linear bearings. The movement of the mounts is easily controlled by a rack and pinion drive. In the current setup, we have the ability to image red (i.e. Texas Red, Alexa-594) and green (i.e. NBD, Alexa-488) dyes and the existing filters can be mixed to provide fluorescence resonance energy transfer imaging (FRET). The filter sets used were larger versions of the standard sets produced by Chroma Technologies for use in epifluorescence microscopes. Our red and green sets correspond to Chroma's sets 41027 and 31001.

Expanding from the design of Ratzlaff, tandem-lens imaging is performed in our experiments between two lenses where the object is placed at the focal length of the first lens and the image is formed at the focal length of the second lens.[221] Figure 4.1 shows a schematic illustration of the imaging strategy with epi-illumination employed in our tandem-lens design. To provide epi-illumination, the light from a 100 W high-pressure

mercury arc lamp was collimated by a lens (L4, f = 17 mm aspheric lens) and passed through an excitation filter (Chroma Technology Corp., Rockingham, VT) onto a holographic diffuser (Edmund Optics, Barrington, NJ). The illuminated holographic diffuser was then imaged into the plane of the sample via a tandem-lens pair, L3 and L1 (85 mm f/1.4 Nikon 35 mm SRL lens and 50 mm f/1.2 Nikon 35mm SRL lens, respectively) with the desired illumination wavelengths reflecting off the dichroic mirror (Chroma Technology Corp., Rockingham, VT) in between them. The emitted fluorescence light from the sample was collected by an objective lens, L1, passed through a dichroic mirror and emission filter, and was then imaged onto a CCD camera by the imaging lens (L2, 50 mm f/1.2 Nikon 35mm SRL lens).

The total internal reflection pathway is shown in figure 4.2. The process of total internal reflection occurs when light propagating through a medium of high refractive index encounters an interface to a second medium of lower refractive index at an angle greater than the critical angle.[214] At the interface, where TIR occurs, an evanescence wave is generated in the second medium and decays exponentially. For supported lipid bilayers solid supports under an aqueous solution, the electromagnetic wave penetrates the glass/buffer interface to approximately a depth of 70 nm,[222] exciting only the fluorophores near or at the surface. TIR illumination is carried out by sliding in a smaller dichroic mirror and beam stop into the epi-illumination beam path immediately after the excitation filter. This diverts the excitation beam down and out of the

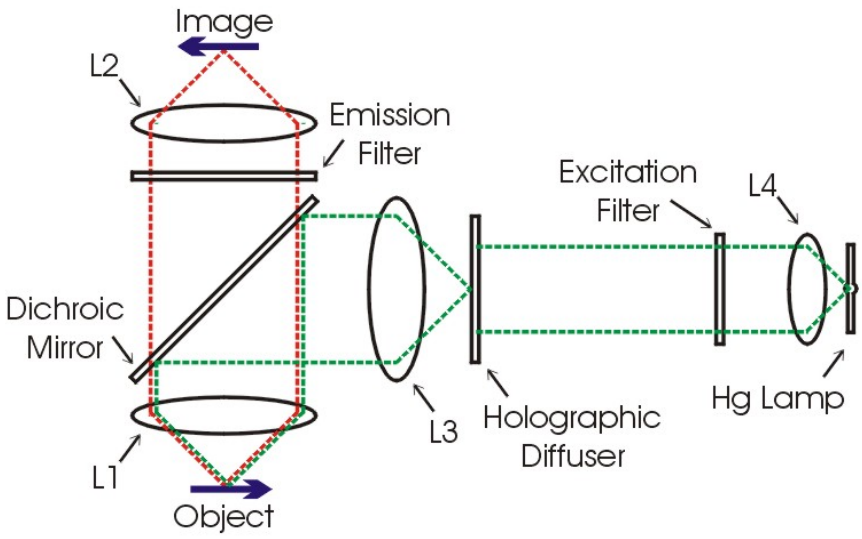

Figure 4.1. Epifluorescence illumination in the macroscope. The collimated light from a mercury arc lamp is passed through the excitation filter and illuminates a holographic diffuser. The illuminated holographic diffuser acts as a source for lens L3, which passes a collimated beam to the dichroic mirror. It is then reflected through lens L1 and an image of the diffuser is formed in the plane of the sample.

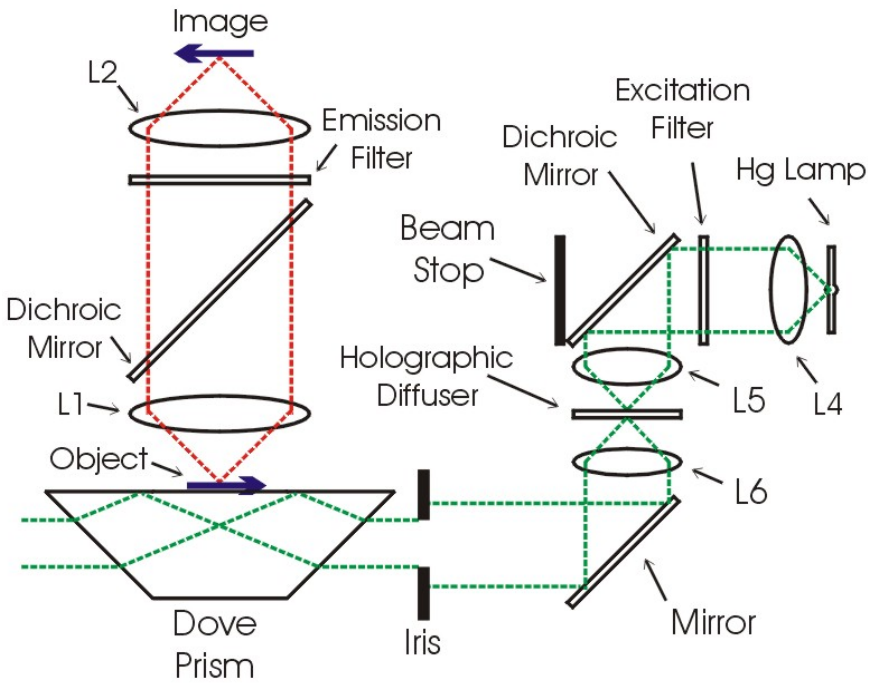

Figure 4.2. TIR illumination in the macroscope. The collimated light from a mercury arc lamp is passed through the excitation filter and reflected off a dichroic mirror through lens L5. Lens L5 forms an image of the arc on the holographic diffuser. The illuminated holographic diffuser acts as source for lens L6, which passes a collimated beam to the aluminum mirror where it is reflected through an iris and into a dove prism. Total internal reflection of the excitation beam occurs at the sample buffer interface, generating an evanescence wave into the sample.

macroscope where it is focused onto a holographic diffuser by lens L5 (50 mm f/1.4 Nikon 35 mm SRL lens). The diffuser is placed approximately at the focal length of lens L6 (f = 30 mm), to produce a collimated illumination beam. This beam is reflected off of an aluminum mirror and passed through an iris before entering a dove prism, where total internal reflection of the beam occurs, allowing for evanescence wave illumination of the sample.

Magnification in a tandem lens system is calculated by the ratio of the focal length of the imaging lens to the objective lens (L2/L1). Since our system uses two 50 mm f/1.2 lenses in tandem, it provides 1x magnification and a numerical aperture of approximately 0.4. A CAD rendering of the EF/TIRF macroscope is shown in Figure 4.3. Data collected from arrays of SLB are corrected for vignetting by dividing the entire image by a standard image. The standard image is acquired by imaging a single SLB with an area greater then the field of view of the macroscope (9 mm x 7 mm). Data can then be collected from the corrected image by averaging the intensity from regions encompassing the areas of each box.

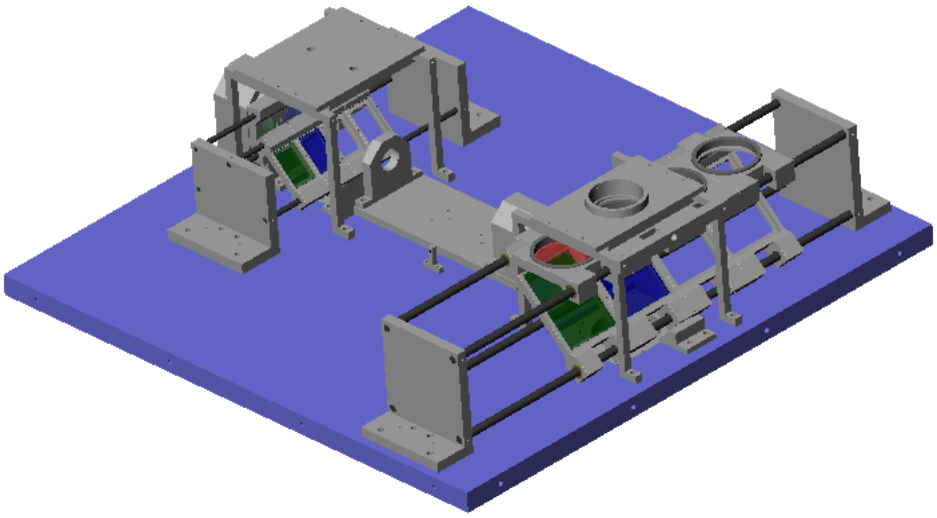

Figure 4.3. EF/TIR macroscope rendering.

Solid Supported Lipid Bilayers

SLBs are produced by the spontaneous fusion of small unilamellar vesicles (SUVs) to a hydrophilic surface such as glass.[68] The production of SUVs is carried out by extruding multilamellar vesicles through polycarbonate filters at high pressures.[73] To do this, lipids mixtures of the desired molar ratios were mixed in chloroform, dried under a stream of nitrogen, desiccated under vacuum for 2 hrs, and reconstituted in 10 mL of pH 7.2 PBS buffer, I = 150 mM with NaCl. The lipid solution was subjected to 10 freeze/thaw cycles in liquid nitrogen to produce multilamellar vesicle dispersions. The multilamellar vesicles were then extruded 5 times through a 50 nm polycarbonate filter. The average diameter of the SUVs was measured to be 82 nm by dynamic light scattering (90 Plus, Brookhaven Instruments Corp., Holtsville, NY).

Array Chip Fabrication

Array fabrication was carried out on chip using standard photolithographic techniques. 1 in^2 microscope cover slips were cleaned by boiling in a 10% 7X detergent solution (ICN, Costa Mesa, CA), annealed at 450°C for 5 hrs, and coated with 1000 Å of chrome by metal evaporation (BOC Edwards Auto 306 Metal Evaporation Chamber, Wilmington, MA). An approximately 6 μm thick photoresist coating was spun onto the chrome coated slides and baked at 90 °C for 45 min in a small oven (Black & Decker). The array chip photomask was designed on CorelDRAW and reduced onto 35 mm film as a negative.[3]. UV illumination through the photomask allowed the development of the photoresist, which created a 10 x 10 array of 0.6 mm x 0.6 mm boxes separated by 0.4 mm hydrophobic photoresist walls. The exposed chrome was then removed using a

commercial chrome etchant, yielding an array of hydrophilic glass plates with hydrophobic photoresist walls.

4.4. Results

In a first set of experiments, we wished to demonstrate that it would be possible to easily scale-up the microcapillary injection method for creating addressed arrays of phospholipid membranes from previous 3 x 3 and 4 x 4 formats.[14] For this purpose, we chose to address a 10 x 10 array of 0.6 mm boxes separated by 0.4 mm hydrophobic walls with alternating vesicle solutions (Figure 4.4). Microcapillary tips were used to deliver vesicle solutions to each unique address on the array. In order to achieve this, capillary tubes were pulled in a micropipette puller to an outer diameter of less than 10 μm. These tips were treated with 1,1,1,3,3,3-hexamethyldisilazane vapor in a 75° C oven to make the surface hydrophobic. This allowed for easy transfer of vesicle solution from the tip to the glass surface. By attaching the pulled capillary to a 100 μL micropipette, the dispensing of droplets to the surface of the array chip could easily be controlled. To perform the addressing, an array chip was placed on a cold plate and the temperature of the chip was adjusted to just above the dew point in order to prevent evaporation of the addressed solutions. A sample of 35 μL was drawn into the tip using the micropipette and pressure on the solution was adjusted until the desired size droplet was dispensed from the tip (~60 nL). The solution was then delivered to the desired location on the array chip and the tip was cleaned before the next solution was introduced. Once the array chip was fully addressed, the chip was submerged in purified water (18 MΩ/cm^2, NANOpure Ultrapure Water System, Barnstead, Dubuque, IA), to

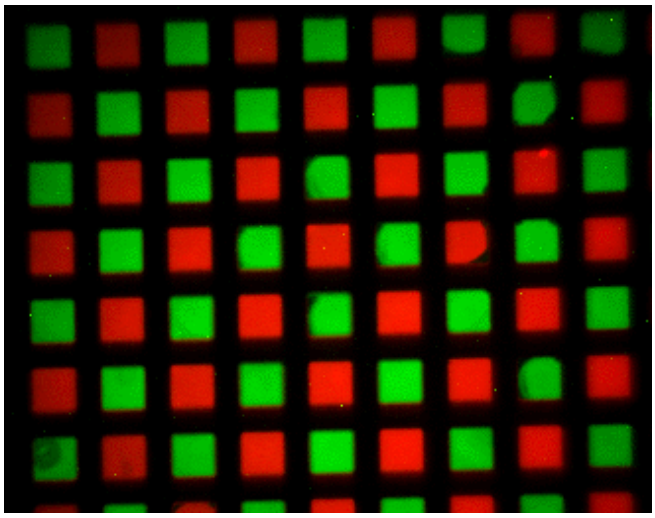

Figure 4.4. Combined images of the array chip addressed with red and green dye labeled SLBs. Each box is 0.6 mm square separated by 0.4 mm hydrophobic walls.

remove excess vesicles. The boxes were addressed with the following solutions: 1% Texas Red 1,2-dihexadecanoyl-*sn*-glycero-3- phosphoethanolamine (Texas Red-DHPE) in egg phosphatidylcholine (Egg-PC), and 5% 1,2-dipalmitoyl-*sn*-glycero-3-phosphoethanolamine-n-(7-nitro-2-1,3-benzoxadiazol-4-yl) (NBD-PE) in egg-PC vesicles to make a two color pattern. It should be emphasized that this array of 63 boxes took only 20 minutes to address. This is a significant advantage when compared to the 1 hour needed to address a 4 x 4 array of smaller boxes.[14,223] Here, we have demonstrated that it is feasible and practical to make large arrays with ease for massively parallel experiments. Only two unique chemistries were alternated in this particular image; however, it should be emphasized that it is nearly as easy to employ many unique lipid compositions as is demonstrated below.

Fluorescent Resonance Energy Transfer Imaging

The FRET process occurs when an acceptor fluorophore is brought within close proximity of a donor fluorophore. If there is sufficient overlap in the emission spectrum of the donor and the absorbance spectrum of the acceptor, then non-radiative energy transfer can occur. This process can accurately measure distances for interactions in the 1-10 nm range.[224] Such distances are important in cellular signaling processes where signaling events occur at cell-cell contact sites. An example of this phenomenon is the behavior of G-protein coupled receptors whereby the an external stimulus causes proteins to rearrange in cellular membranes in order to facilitate a signaling processes.[225] Cell-cell adhesion and protein helix interactions can be followed in model systems using fluorescence resonance energy transfer (FRET). [226,227] As a demonstration of this

process, we monitored the FRET interactions between NBD-PE and Texas Red-DHPE in SLBs.

Total internal reflection FRET with the EF/TIRF macroscope was carried out by combining the green dye excitation filter and dichroic mirror (exciting with 475-500 nm) with the red dye emission filter and a dichroic mirror (observing at 600-660 nm). A unique advantage of our macroscope setup is the ability to easily mix and match excitation and emission filters (Figure 4.3). A 6 x 6 section of the array chip was addressed with thirty six unique SLB chemistries and then imaged (Figure 4.5). Along one axis, the mole fraction of Texas Red-DHPE in the SLBs was varied from 0 to 1.0 mol percent and along the other, the mole fraction of NBD-PE was varied from 0 to 5.0 mol percent. Fluorescent images of the chip in the red, green and FRET channels are shown in figure 4.5 A, B, and C respectively. 3D plots of the normalized fluorescence intensity vs. the mole percent of each dye present in the respective membranes are shown under their corresponding images in figures 4.5.D (red), 4.5.E (green), and 4.5.F (FRET). As the mole fraction of Texas Red-DHPE was increased, the fluorescence intensity observed was unaffected by the presence of the NBD-PE when the chip was illuminated with green light and imaged in the red (figure 4.5.D). As both the mole fraction of Texas Red-DHPE and NBD-PE increased, the fluorescence intensity from the NBD decreased due to the FRET process upon blue excitation (figure 4.5.E). Conversely, as we increased the concentration of donors and acceptors we observed an increase in fluorescence emitted from the Texas Red when the NBD was excited. In our given concentration ranges, the maximum FRET occurs in the 5% NBD, 1% Texas Red box. We can calculate the efficiency (E) of the FRET process (equation 1) occurring in

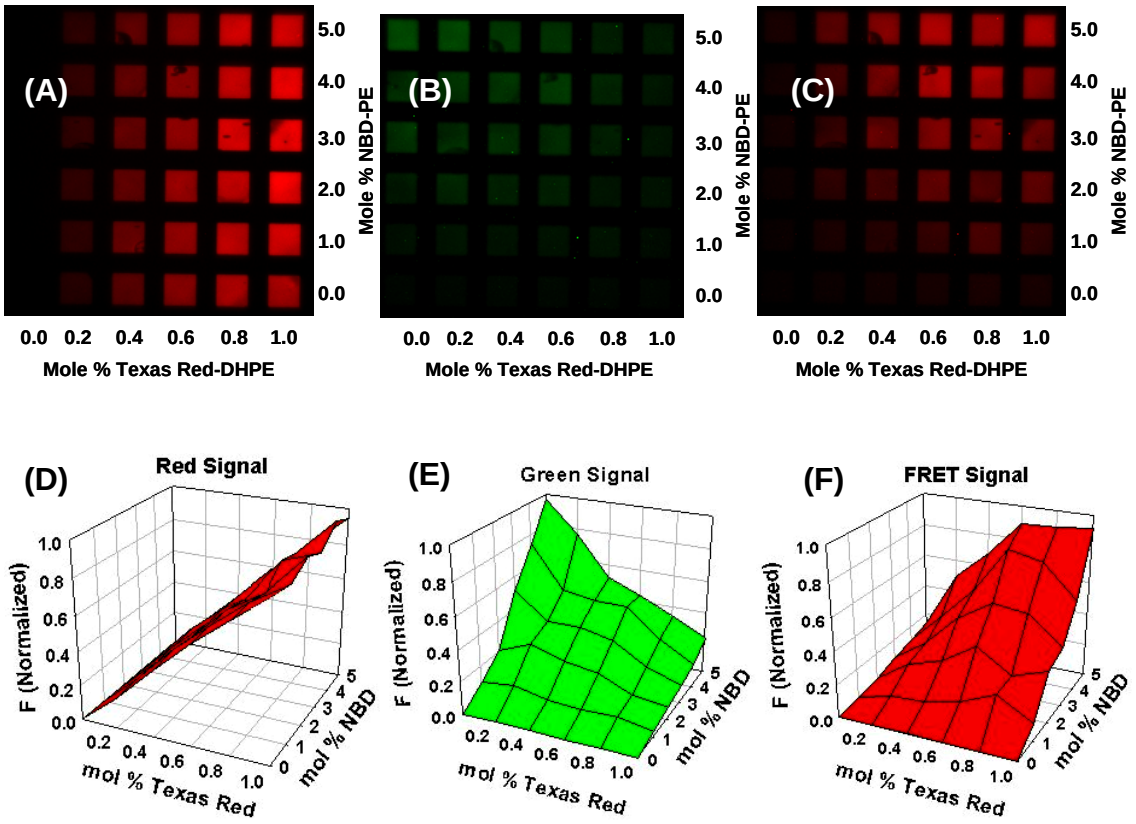

Figure 4.5. Images and data from the FRET experiment. Each sample box is 0.6 mm square. (A) Red fluorescence image. (B) Green fluorescence image. (C) FRET fluorescence image. (D) Plot of the normalized fluorescence intensity from the red image. As the mole fraction of Texas Red-DHPE increases in the membrane the fluorescence intensity increase is unaffected by the presence of NBD-PE. (E) Plot of the normalized fluorescence intensity from the green image. As the mole fraction of Texas Red-DHPE increases in the membrane, the fluorescence intensity of NBD-PE is quenched by the Texas Red-DHPE. (F) Plot of the normalized fluorescence intensity from the FRET image. As the mole fraction of Texas Red-DHPE and NBD-PE increases in the membrane, the fluorescence intensity observed from the FRET process increases.

this box using its average intensity, F_{DA}, and the intensity from the 5% NBD, 0% Texas Red box, F_D.

Equation 1: $$E = 1 - F_{DA} / F_D$$

The Förster radius (R_o) for the NBD - Texas Red pair in a lipid membrane is 7.25 nm.[228] Using the Förster radius and the efficiency we can calculate the dye spacing in the membrane (R) using equation 2.[224]

Equation 2: $$E = \frac{R_o^6}{R_o^6 + R^6}$$

From our data we calculated the spacing of the lipids in the 5% NBD, 1% Texas Red box to be 5.9 nm.

Ligand Density Arrays

Knowing the saturation point of proteins on the surface of lipid membranes is important for several reasons. First, it allows for an approximate measurement of the footprint of a protein bound to a membrane. It is also useful for quantitative measurements of the amount of a protein bound at the surface. This is particularly useful for investigating enzyme kinetics of surface bound enzymes.[16] As a demonstration of the ability to measure protein footprints at the membrane interface in a high throughput fashion, a simple binding experiment was preformed. Vesicle solutions containing 10 mol% 1,2-dipalmitoyl-*sn*-glycero-3-phosphoethanolamine-n-(2,4-dinitrophenyl) (DNP-PE) in egg-PC, 10% 1,2-dioleoyl-*sn*-glycero-3-phosphoethanolamine-n-(biotinyl) (biotin-PE) in Egg-PC, and pure Egg-PC were combined to create vesicle solutions ranging from 0-5 mole percent of the respective

ligands. These solutions were mixed to the desired mole ratio and addressed onto a single array chip with eighteen unique chemical compositions. After vesicle fusion, the array chip was rinsed with pH 7.2 PBS buffer and incubated with a 0.1 mg/mL bovine serum albumin (BSA) solution for 30 min. It was rinsed again with PBS buffer and incubated with a solution containing 4 μM Alexa-594 labeled anti-DNP and 4 μM Alexa-488 labeled streptavidin for 3 hours. The chip was imaged with the EF/TIRF macroscope and the separate red and green images from two different areas of the chip are shown in Figure 4.6. The green image (figure 4.6.A) shows the binding of the Alexa-488 labeled streptavidin and the red image (figure 4.6.B) shows the binding of the Alexa-594 labeled anti-DNP. Linescans across the array chip in the regions highlighted with a white doted line box are shown in figure 4.6.C for the green image and figure 4.6.D for the red image. As can be seen, the anti-DNP reaches its maximum surface coverage sooner then the streptavidin due to its larger size. We note that the maximum surface coverage for the ligand-receptor pairs occur around 3 mole percent for streptavidin and around 2 mole percent for anti-DNP. Assuming that (a) the molecular area of a lipid is ~0.60 nm^2, (b) bivalent binding occurs, and (c) the ligands are distributed equally to both the upper and lower leaflet, we estimate that the footprints of streptavidin and anti-DNP bound on the surface to be 40 nm^2 and 60 nm^2 respectively. This is consistent with literature data from crystal structures of these proteins (34 nm^2 for streptavidin[229] and 60 nm^2 for anti-DNP[230]).

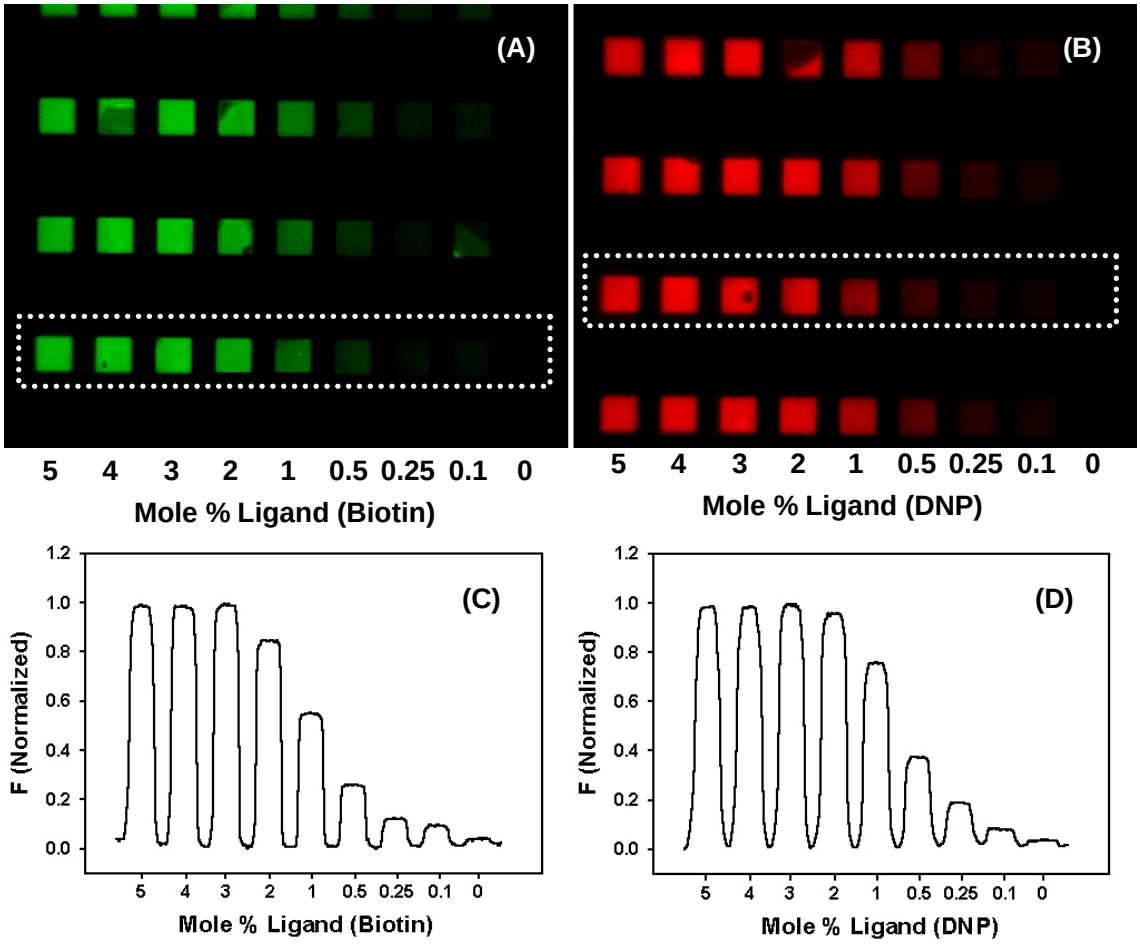

Figure 4.7. Images of a single chip two protein binding assay. Each sample box is 0.6 mm square. Decreasing mole fractions of the two ligands, DNP and biotin, were addressed from left to right. (A) Green channel showing the binding of Alexa-488 labeled Streptavidin. (B) Red channel showing the binding of Alexa-594 labeled Anti-DNP. (C) Linescan across highlighted boxes in (A). (D) Linescan across highlighted boxes in (B).

4.5. Discussion

Total internal reflection fluorescence imaging as well as epifluorescence imaging is important for the investigation of lipid membrane interactions with aqueous analytes. A large array format allows the cholesterol content, ligand density, lipid headroup, alkyl chain, and membrane charge to be modulated in a single on-chip format. Epifluorescence allows the membrane to be imaged in the absence of bulk fluorescence. This should be useful in an array-based format for monitoring two-dimensional protein crystallization of membrane bound proteins as a function of lipid bilayer chemistry. One could also monitor the interactions of several labeled species within the membrane as their concentrations as well as the surrounding membrane composition is altered.

Total internal reflection techniques can be employed for monitoring ligand-receptor binding between membrane bound ligands and aqueous proteins. This is especially important with fluid lipid bilayers for multivalent ligand-receptor interactions. In this case the species within the membrane are free to reorganize in two-dimensions to optimize binding interactions. Such binding events are prevalent in biological processes such as bacterial and viral attacks, human immune response, and signal transduction.[231] One could even monitor the stimulation of T-cells over a lipid bilayer array with various concentrations of GPI-linked signaling moieties at each address. By varying the concentration of ligand, this assay would enable the rapid determination of the minimum concentration for cell signaling.

FRET imaging of large membrane arrays will be useful for investigating processes that occur in cellular membranes where changes in small distances can be observed. This is beneficial for exploring such phenomena as lipid raft formation,

protein-protein interactions, and protein folding. Again, all these process can be studied in an array-based assay by varying a wide variety of membrane constituents.

The number of samples we are currently able to address is limited by the hand addressing techniques being utilized. If combined with existing robotic addressing technologies,[210] the high throughput capabilities of the EF/TIRF macroscope could greatly be enhanced. More samples per chip would not only allow the rapid collection of larger quantities of data but also larger numbers of duplicate samples, increasing the quality of the data.

CHAPTER V

AN IMPROVED ARRAY CHIP AND ADDRESSING TECHNIQUE

5.1. Synopsis

Within this chapter is presented the design and fabrication of a new silicon/glass array chip and addressing apparatus. It was found that using this equiptment greatly increases the yield of successfully addressed chips. It was also determined that the new chip in conjunction with the new addressing apparatus greatly decreases the amount of time required to address an entire array.

5.2. Introduction

One of the major limitations of carrying out large scale experiments as outlined in the previous chapter is the array chip itself. The addressing of such a system without the aid of robotic printing and environmental temperature and humidity control is extremely challenging. Its shallow walls, approximately 6 microns deep with a 0.6 mm square base, has a volume of only 2 nL. This means that any droplet large enough to span the surface must also protrude above the box exposing a large surface area of the droplet to the open air environment. Even though the droplets are addressed onto an array chip which is under temperature control, a sudden change in the room environment

can cause the drops to either swell into one another or evaporate, both of which render the array unusable.

The method of addressing from a modified micropipette/pulled capillary has limitations also. Because the method involves the use of air pressure to dispense the droplets and air is a compressible fluid, the delivered droplet volume is hard to control. Often times this leads to either over filling or under filling of a given well. While under filling presents a minimal problem, overfilling a well while addressing the array chip typically results in the solution spilling over into several adjacent wells and ruins the entire chip. Also, the apparatus design did not allow for rapid changing of tips which meant that the tip needs to be cleaned between each solution being addressed wasting large amounts of time.

Finally, it would be of great advantage if the array chip could be reused. This would save on time spent fabricating chips and make up for the fact that it requires many array chips to produce one good sample due to the low yields that the addressing process provides. The current materials used in fabricating the array chip, namely photoresist, chrome, and glass do not allow for the array chip to be cleaned and reused.

The desire to fabricate an array chip with deeper wells in order to increase the well volume and overcome overfilling problems required a change in materials. The floor of the wells needs to remain glass in order to allow for the formation of supported lipid bilayers as well as TIR illumination. This left few materials of choice which could be fabricated in a small enough pattern and sealed to the glass to provide the desired wells. One such material is crystalline silicon. Crystalline silicon, as used in the

semiconductor industry, is widely available, has well established procedures for bulk micromachining, and is easily bonded to silica or Pyrex substrates.[164] In the following text we present a new array chip fabricated in silicon and glass and a novel means to rapidly hand dispense precise amounts of solution to its wells.

5.3. Methods and Materials

Materials

Silicon <100>, P-type, double-side polished,100 mm diameter, 375 micron thick, wafers, coated with 100 nm of CVD silicon nitride were supplied by Montco Silicon Technologies Inc. (Spring City, PA). Polished Pyrex 7740 wafers, 1 in. square were purchased from Precision Glass and Optics (Santa Ana, CA). Microposit S1813 positive photoresist and Microposit developer were obtained from Rohm and Haas Electronic Materials (Marlborough, MA). Potassium hydroxide, 200 proof ethanol, phosphoric acid, 30 % peroxide, hydrochloric acid, hydrofluoric acid, ammonium hydroxide, sodium phosphate, and sodium chloride were used as received from Sigma-Aldrich (Saint Louis, MO). Purified water was obtained with a resistance of 18 MΩ/cm^2, (NANOpure Ultrapure Water System, Barnstead, Dubuque, IA). Teflon flangeless ferrules (P-200N), 1/4”-28 female slip-type luer adapter (P-628), and 1/4”-28 short Teflon flangeless nuts (P-218X) were purchased from Upchurch Scientific (Oak Harbor, WA). 10 μL LX gastight syringe and repeating dispenser were acquired from Hamilton (Reno, NV). Capillary tubes, 1.5 mm O.D. were supplied by World Precision Instruments (Sarasota, FL). Texas Red 1,2-dihexadecanoyl-*sn*-glycero-3-

phosphoethanolamine (Texas Red-DHPE) was purchased from Invitrogen (Carlsbad, CA). Egg phosphatidylcholine (Egg-PC) and 1,2-dipalmitoyl-*sn*-glycero-3-phosphoethanolamine-n-(7-nitro-2-1,3-benzoxadiazol-4-yl) (NBD-PE) were acquired from Avanti Polar Lipids (Alabaster, AL).

Silicon/Glass Chip Fabrication

The array chip photomask was designed on CorelDraw and reduced into a 35 mm film as a negative.[3]. The photomask consisted of an 8 x 6 array of 0.9 mm square boxes separated by 0.2 mm spacings. Several negatives were taped to a 5 in. square piece of window glass with double-side tape(Acme Glass Co., College Station, TX) and the spaces between negatives was filled in with black electrical tape. This produced a large photomask enabling 9 devices to be fabricated out of one wafer. Approximately 6 μm of Microposit photoresist is spun onto the silicon wafer and baked at 90 °C for 45 min in a toaster oven (Black & Decker). The photomask was aligned with the crystal planes in a way such that the sides of the boxes would be parallel to the flats on the silicon wafer. This insures that the walls of the wells to be etched into the silicon will be parallel to the <110> plane in the wafer. The photoresist was exposed to UV light from a Quintel Q400MA mask aligner (San Jose, CA) for 1 min. Next the photoresist was developed in Microposit developer until the underlying silicon nitride layer was exposed in the patterned areas. The wafer was then dipped in a 10% solution of hydrofluoric acid for 30 sec. and rinsed with copious amounts of purified water (CAUTION: HF is extremely dangerous and should be handled with the utmost care and respect. When working with

HF a face shield, lab coat, and gloves should be worn at all times.). Immediately following this step the wafer was etched in a March Plasma Systems Model CS-1701 reactive ion etcher (Concord, CA) for 500 seconds at a power of 150 W with of a flow rate of 5 cm^3/s of tetrafluoromethane. Next the wafer is again dipped in a 10 % solution of hydrofluoric acid for 2 min. to ensure the removal of the small SiO_2 layer which resides below the silicon nitride layer and rinsed with copious amounts of purified water. The photoresist was then stripped from the wafer using acetone. Next the wafer was placed in a homemade wet etching station consisting of a 2 L reaction kettle (Fisher Scientific, Houston, TX), a condenser and a Teflon wafer dipper (Entegris, Chaska, MN). Figure 5.1 is a photograph of the assembled homemade wet etching station. The wafer was allowed to reflux in the etching bath, 1.5 L of 40 % KOH solution at 85° C (600 g KOH, 300 mL ethanol, 1200 mL purified water), until the wells were completely etched through the wafer (approximately 4.5 hrs.). After extensive rinsing with copious amounts of purified water, the wafer was scribed and broken into 9 individual silicon chips. These chips were placed in a ceramic boat and boiled in concentrated phosphoric acid for 2 hrs. completely removing the silicon nitride layer. After extensive rinsing, the chips along with 9 Pyrex wafers were cleaned using the RCA cleaning method.[232] In short, the chips were placed in an 80° C bath of 5:1:1 ratios of water, 30 % peroxide, and ammonium hydroxide for 10 min., followed by extensive rinsing. Next the silicon chips are placed in a 10 % solution of hydrofluoric acid for 2 min. and rinsed again. Then both the silicon chips and the Pyrex wafers were placed in an 80° C bath of

Figure 5.1. Photograph of the assembled homemade wet etching station built from a 2 L reaction kettle, condenser, and a Teflon wafer dipper.

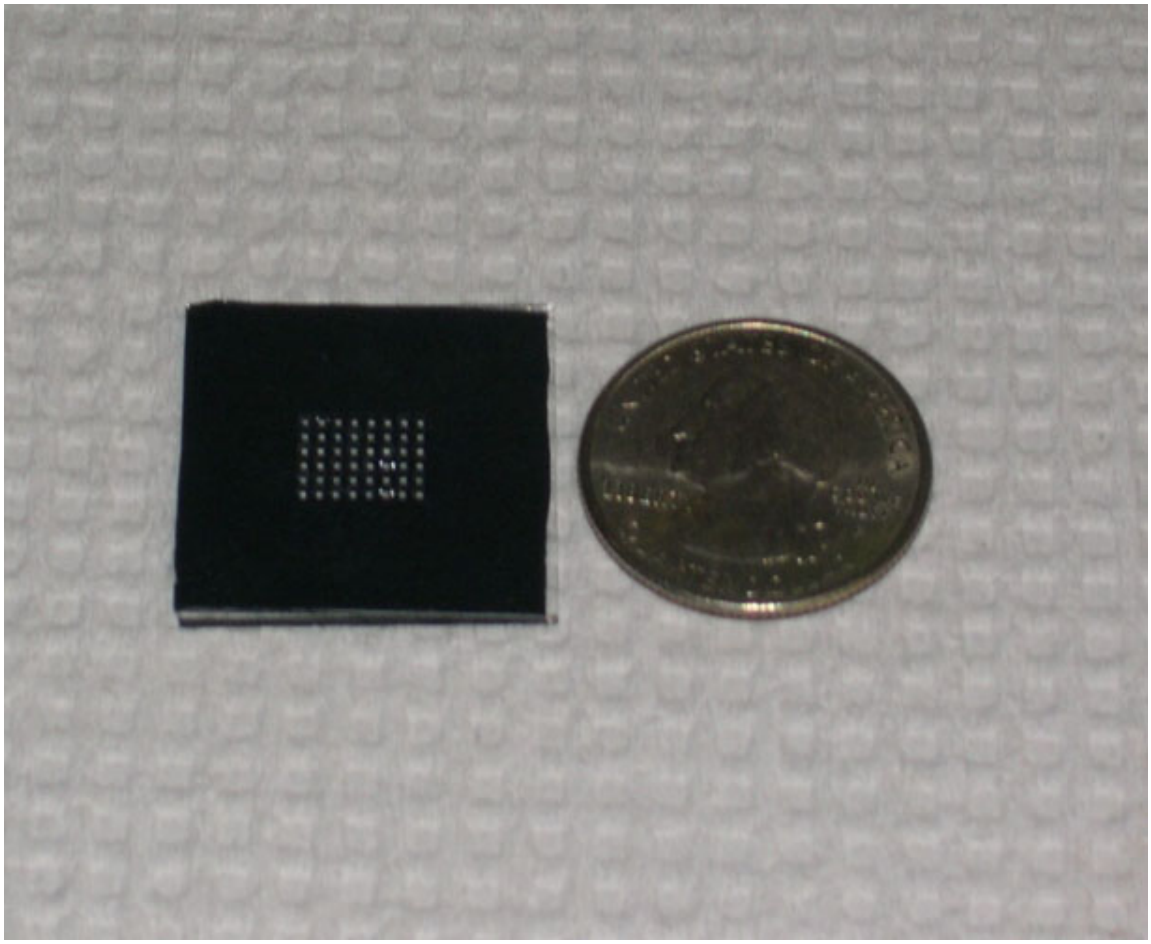

Figure 5.2. Photograph of a completed 1 in. square silicon/glass array chip. A quarter is shown next to the chip for size perspective.

6:1:1 ratios of water, 30 % peroxide, and hydrochloric acid for 10 min. After rinsing with purified water and drying under a stream of nitrogen gas, the silicon chips and the Pyrex wafers were anodically bonded together to form the array chip.[164] The anodic bonding conditions were 1000 V, 1mA, 375° C for 3 min. Figure 5.2 shows a completed silicon/glass array chip.

Rapid Addressing Apparatus

Tips were prepared by pulling the 1.5 mm O.D. capillary tubes as described in the previous chapter. The tips were cut to a length of 35 mm and assembled with a slip-type luer adapter, ferrule, and flangeless nut as illustrated in figure 5.3. The 10 μL syringe was outfitted with the repeat dispenser. This setup allows for push button delivery of $1/50^{th}$ of the maximum volume of the syringe providing us with the ability to reproducibly dispense 200 nL from a 10 μL syringe. Figure 5.4 shows the assembled addressing apparatus.

Preparation of Vesicle Solutions

The production of small unilaminar vesicles (SUV) is carried out by means of extruding multilamellar vesicles through polycarbonate filters at high pressures.[73] To do this, lipids mixtures 2 % Texas Red-DHPE in Egg-PC and 5 % NBD-PE in Egg-PC are dried under vacuum for 2 hrs and reconstituted in 10 mL of pH 7.2 PBS buffer, I = 150 mM with NaCl. The lipid solutions are then subjected to 10 freeze/thaw cycles in liquid nitrogen to produce multilamellar vesicle dispersions. The multilamellar vesicle

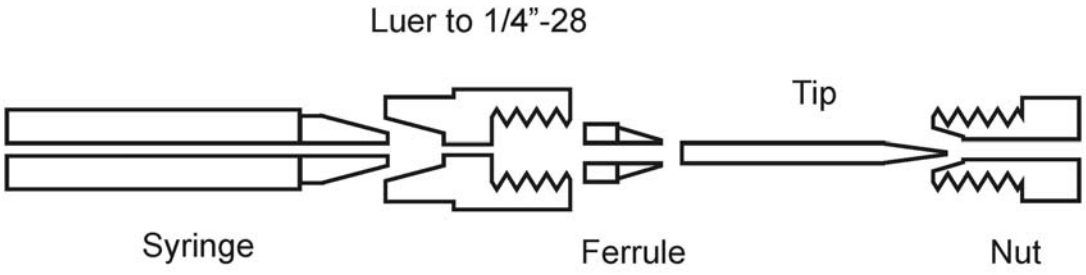

Figure 5.3. Cutaway exploded view of rapid change tip assembly.

Figure 5.4. Photograph of the assembled addressing apparatus with luer lock tip assembly.

solutions are then extruded 5 times through a 50 nm polycarbonate filter. The average diameters of the SUVs were measured to be 84 nm for Texas Red-DHPE and 82 nm for NBD-PE by dynamic light scattering (90 Plus, Brookhaven Instruments Corp., Holtsville, NY).

5.4. Results and Discussion

In order to test the new array chip and addressing apparatus, the addressing of every other well with alternating lipid vesicle solutions was undertaken. After addressing the wells with the 2 % Texas Red-DHPE and the 5 % NBD-PE solutions, the entire chip was submerged in purified water and covered with a microscope cover slip. This prevents the supported bilayer array from drying and being destroyed during imaging. Figure 5.5 shows both the green and red false color images of the array taken by the EPI/TIR macroscope. It is noted that the number of trials to complete the array was only 4. This is approximately a 10 fold reduction in the number of trials needed to complete the combined array using the previous method. Not only does the new chip and addressing process drastically increase the yield of successful addressing attempts, they also drastically reduce the time to address each chip. This is mostly accomplished by the combination of the deeper wells with the dispensing accuracy of the new addressing apparatus. In fact, the loss of a partially addressed chip due to the overfilling of wells has almost been completely eliminated. Another benefit is the ability to rapidly change tips during addressing. By having an individual tip for each sample, the cleaning step between droplet deliveries is eliminated. This savings in time greatly adds up as the

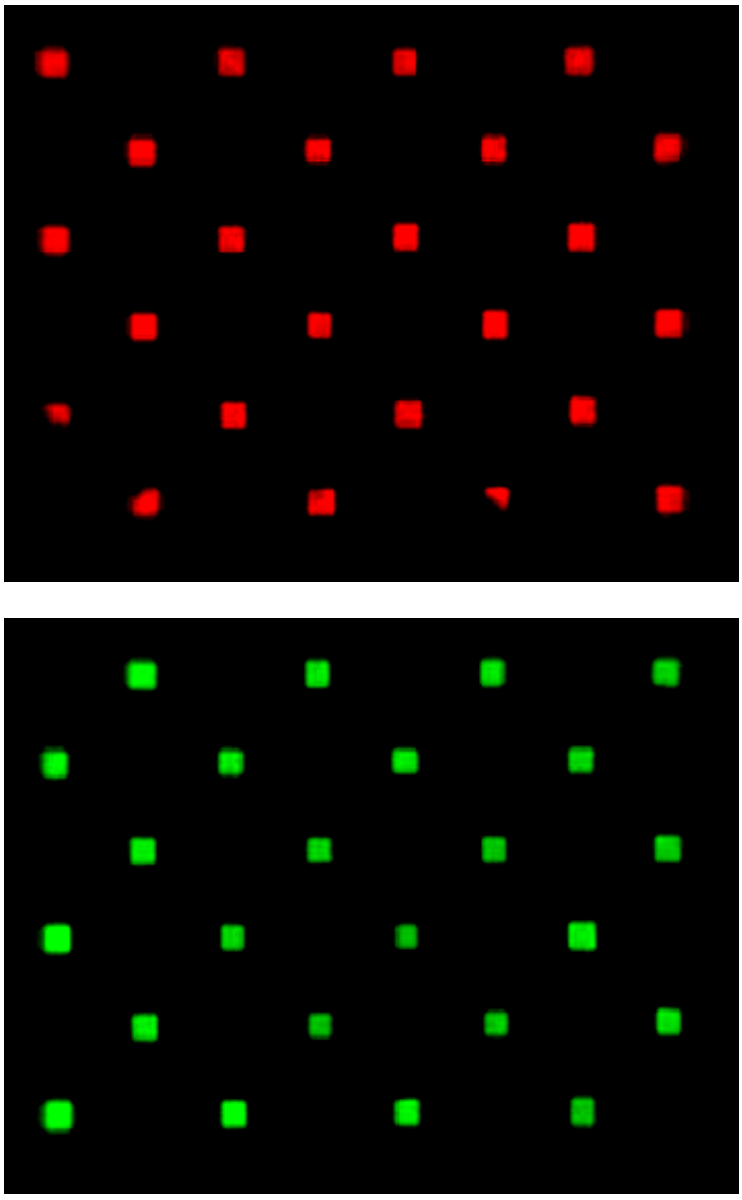

Figure 5.5. Red and green false color images of the silicon/glass array chip addressed with alternating solutions of 2 % Texas Red-DHPE (red image) and 5 % NBD-PE (green image). The boxes are ~ 250 microns.

number of different samples being addressed is increased. In the previous method of addressing, the amount of time spent cleaning the tip and preparing it to deliver the correct size droplet was far greater then the time spent actually delivering droplets to the chip. It was estimated that for a chip with 16 different samples, the amount of time required to complete addressing an entire chip is reduced to 1/5 the time it takes to address using the old methods.

Unfortunately the goal of a reusable array chip has not been realized. It was found that repeated use of the array chips results in poor quality SLB arrays. A false color image of a 2 x 2 section of a reused array chip addressed with 5 % NBD-PE is shown in figure 5.6. This problem is most likely occurring due to the glass surface being damaged during addressing with the glass tip. Current studies are underway to find a replacement tip material which will not damage the array chip.

5.5. Conclusions

Here we have presented a means in which to fabricate a new array chip out of silicon and glass and a novel addressing method using a repeat dispenser, syringe and a rapid change tip system. Both of these have greatly increased the yield of successfully addressed arrays and greatly decreased the arraying time. Due to the large amount of time spent on fabricating the array chips, either mass production of the chips or a reusable chip will need to be developed in order to make this a viable platform for use in conjunction with the EPI/TIR macroscope.

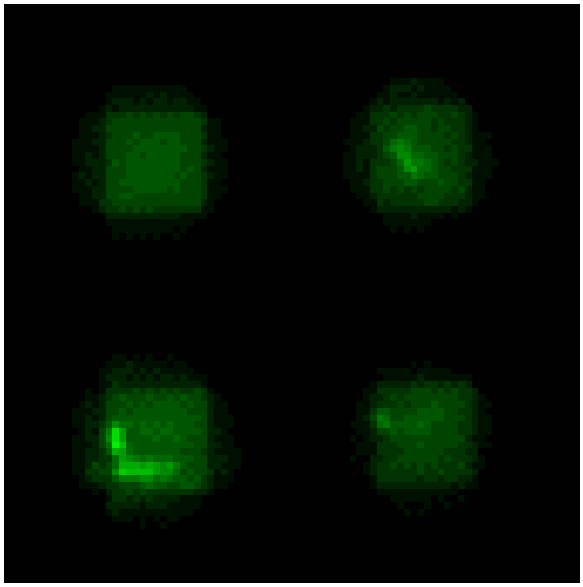

Figure 5.6. False color image of a 2x2 section of a poor quality SLB array resulting from multiple uses of an array chip. The boxes are ~250 microns.

CHAPTER VI

SUMMARY AND CONCLUSIONS

In this dissertation a novel method of depositing metallic nanoparticle films inside sealed microfluidic devices is presented along with the development and construction of an epifluorescence/total internal reflection macroscope. In conjunction with the EPI/TIR macroscope, an array-based system was also developed for producing large scale arrays of solid supported phospholipid bilayers.

The patterning of metal nanoparticle films inside sealed microfluidic devices should indubitably enhance the rapid prototyping capabilities of soft lithography. It provides the ability to rapidly design and test a variety of microfluidic devices with different surface chemistries from a single microfluidic system. This can be achieved through the patterning of different geometries of metal nanoparticle films on the micron scale through the use of photomasks and controlling the surface morphology of the metal nanoparticle films on the nanoscale by controlling the solution conditions.

Here we presented a means to pattern any desired geometry inside of sealed microchannels with TiO_2 floors. The process is carried out through the deposition of metal ions in aqueous solution onto the TiO_2 surface through photoreduction. Due to the backside illumination method employed in this process, this technique is currently limited to the patterning of 6 micron features. This minimum resolution could be reduced through the use of a high precision projection lithography system.

Control over the nanoscale morphology of the films was demonstrated by controlling the solution pH during the deposition of the metal nanoparticle films. It was observed that the densest films with the smallest particles formed at a pH of 5 and the density of the films decreased while the size of the particles increased as the pH was lowered. Also, as the pH was increased the particle size increased and the film retained a high density. This is explained by a change in surface charge of the TiO_2 film. At lower pH's, the surface is more positively charged which means that there are less sites for metal ion adsorption which decreases the density of the films.

The utility of these nanoparticle films to present different surface chemistries within the channels was demonstrated. This was achieved by fabricating a sensor device inside sealed microchannels consisting of two patches of metal nanoparticles addressed with different PEG thiol monolayers. The monolayers presented a different ligand at each nanoparticle patch allowing for the capture of different proteins from solution at each location.

The ability to perform high numerical aperture, large area imaging allows for the combination of high throughput screening with the advantage of one-shot imaging. Combining this with large arrays of solid supported bilayers allows for the investigation of important cellular processes, which occur in cellular membranes. Examples of such systems are cellular signaling, viral attack and entry, and ligand-receptor binding events.

The EPI/TIRF macroscope presented within this thesis has been shown to be useful in imaging large arrays of solid supported phospholipid bilayers. Arrays of phospholipid bilayers with varying amounts of membrane components were imaged. It

has been useful for imaging protein binding experiments where two different ligand arrays of varying ligand concentration were presented on the same chip. The EPI/TIR macroscope has also proven to be useful for fluorescence resonance energy transfer studies by imaging a two component, two-dimensional dye concretion array.

Finally an improved array chip and addressing method was presented to increase the efficiency of the bilayer array making process. While the new chip is not recyclable, if mass-produced with the proper facilities, it will make an excellent platform for use with the EPI/TIRF macroscope.

REFERENCES

(1) Plant, A. L.; Brighamburke, M.; Petrella, E. C.; Oshannessy, D. J. *Analytical Biochemistry* **1995**, *226*, 342-348.

(2) Pum, D.; Stangl, G.; Sponer, C.; Riedling, K.; Hudek, P.; Fallmann, W.; Sleytr, U. B. *Microelectronic Engineering* **1997**, *35*, 297-300.

(3) Yang, T. L.; Jung, S. Y.; Mao, H. B.; Cremer, P. S. *Analytical Chemistry* **2001**, *73*, 165-169.

(4) Yang, T. L.; Baryshnikova, O. K.; Mao, H. B.; Holden, M. A.; Cremer, P. S. *Journal of the American Chemical Society* **2003**, *125*, 4779-4784.

(5) Xu, L.; Frederik, P.; Pirollo, K. F.; Tang, W. H.; Rait, A.; Xiang, L. M.; Huang, W. Q.; Cruz, I.; Yin, Y. Z.; Chang, E. H. *Human Gene Therapy* **2002**, *13*, 469-481.

(6) Ono, A.; Freed, E. O. *Proceedings of the National Academy of Sciences of the United States of America* **2001**, *98*, 13925-13930.

(7) Kasahara, K.; Sanai, Y. *Trends in Glycoscience and Glycotechnology* **2001**, *13*, 587-594.

(8) Stoddart, A.; Dykstra, M. L.; Brown, B. K.; Song, W. X.; Pierce, S. K.; Brodsky, F. M. *Immunity* **2002**, *17*, 451-462.

(9) Qi, S. Y.; Groves, J. T.; Chakraborty, A. K. *Proceedings of the National Academy of Sciences of the United States of America* **2001**, *98*, 6548-6553.

(10) Muller, P.; Rudin, D. O.; Ti Tien, H.; Wescott, W. C. *Nature* **1962**, *194*, 979-980.

(11) Muller, P.; Rudin, D. O.; Ti Tien, H.; Wescott, W. C. *J Phy Chem* **1963**, *67*, 534-535.

(12) Tamm, L. K.; McConnell, H. M. *Biophysical Journal* **1985**, *47*, 105-113.

(13) Groves, J. T.; Ulman, N.; Boxer, S. G. *Science* **1997**, *275*, 651-653.

(14) Cremer, P. S.; Yang, T. L. *Journal of the American Chemical Society* **1999**, *121*, 8130-8131.

(15) Groves, J. T.; Mahal, L. K.; Bertozzi, C. R. *Langmuir* **2001**, *17*, 5129-5133.

(16) Mao, H. B.; Yang, T. L.; Cremer, P. S. *Analytical Chemistry* **2002**, *74*, 379-385.

(17) Kam, L.; Boxer, S. G. *Langmuir* **2003**, *19*, 1624-1631.

(18) Kam, L.; Boxer, S. G. *Journal of the American Chemical Society* **2000**, *122*, 12901-12902.

(19) Spinke, J.; Yang, J.; Wolf, H.; Liley, M.; Ringsdorf, H.; Knoll, W. *Biophysical Journal* **1992**, *63*, 1667-1671.

(20) Sackmann, E. *Science* **1996**, *271*, 43-48.

(21) Zhang, L. Q.; Longo, M. L.; Stroeve, P. *Langmuir* **2000**, *16*, 5093-5099.

(22) Shen, W. W.; Boxer, S. G.; Knoll, W.; Frank, C. W. *Biomacromolecules* **2001**, *2*, 70-79.

(23) Elender, G.; Kuhner, M.; Sackmann, E. *Biosensors & Bioelectronics* **1996**, *11*, 565-577.

(24) Baumgart, T.; Offenhausser, A. *Langmuir* **2003**, *19*, 1730-1737.

(25) Beyer, D.; Elender, G.; Knoll, W.; Kuhner, M.; Maus, S.; Ringsdorf, H.; Sackmann, E. *Angewandte Chemie-International Edition in English* **1996**, *35*, 1682-1685.

(26) Hausch, M.; Zentel, R.; Knoll, W. *Macromolecular Chemistry and Physics* **1999**, *200*, 174-179.

(27) Naumann, C. A.; Prucker, O.; Lehmann, T.; Ruhe, J.; Knoll, W.; Frank, C. W. *Biomacromolecules* **2002**, *3*, 27-35.

(28) Naumann, R.; Schmidt, E. K.; Jonczyk, A.; Fendler, K.; Kadenbach, B.; Liebermann, T.; Offenhausser, A.; Knoll, W. *Biosensors & Bioelectronics* **1999**, *14*, 651-662.

(29) Seitz, M.; Ter-Ovanesyan, E.; Hausch, M.; Park, C. K.; Zasadzinski, J. A.; Zentel, R.; Israelachvili, J. N. *Langmuir* **2000**, *16*, 6067-6070.

(30) Seitz, M.; Wong, J. Y.; Park, C. K.; Alcantar, N. A.; Israelachvili, J. *Thin Solid Films* **1998**, *329*, 767-771.

(31) Plant, A. L. *Langmuir* **1993**, *9*, 2764-2767.

(32) Plant, A. L. *Langmuir* **1999**, *15*, 5128-5135.

(33) Wetzer, B.; Pum, D.; Sleytr, U. B. *Journal of Structural Biology* **1997**, *119*, 123-128.

(34) Bayley, H. *Journal of Cellular Biochemistry* **1994**, *56*, 168-170.

(35) Schuster, B.; Pum, D.; Sara, M.; Braha, O.; Bayley, H.; Sleytr, U. B. *Langmuir* **2001**, *17*, 499-503.

(36) Berquand, A.; Mazeran, P. E.; Pantigny, J.; Proux-Delrouyre, V.; Laval, J. M.; Bourdillon, C. *Langmuir* **2003**, *19*, 1700-1707.

(37) Proux-Delrouyre, V.; Elie, C.; Laval, J. M.; Moiroux, J.; Bourdillon, C. *Langmuir* **2002**, *18*, 3263-3272.

(38) Proux-Delrouyre, V.; Laval, J. M.; Bourdillon, C. *Journal of the American Chemical Society* **2001**, *123*, 9176-9177.

(39) Tampé, R.; Dietrich, C.; Gritsch, S.; Elender, G.; Schmitt, L. In *Nanofabrication and biosystems: integrating materials science, engineering, and biology*; Hoch, H. C., Jelinsk, L. W., Craighead, H. G., Eds.; Cambridge University Press: Cambridge, 1996, pp 201-221.

(40) Ti Tien, H.; Ottova-Leitmannova, A. *Membrane biophysics: as viewed from experimental bilayer lipid membranes (planar lipid bilayers and spherical liposomes)*; 1st ed.; Elsevier: Amsterdam, 2000.

(41) Montal, M.; Mueller, P. *Proceedings of the National Academy of Sciences of the United States of America* **1972**, *69*, 3561-3566.

(42) Bamberg, E.; Alpes, H.; Apell, H. J.; Bradley, R.; Harter, B.; Quelle, M. J.; Urry, D. W. *Journal of Membrane Biology* **1979**, *50*, 257-270.

(43) Gomezlagunas, F.; Pena, A.; Lievano, A.; Darszon, A. *Biophysical Journal* **1989**, *56*, 115-119.

(44) Van Gelder, P.; Dumas, F.; Winterhalter, M. *Biophysical Chemistry* **2000**, *85*, 153-167.

(45) Bezrukov, S. M.; Vodyanoy, I. *Biophysical Journal* **1993**, *64*, 16-25.

(46) Gu, L. Q.; Braha, O.; Conlan, S.; Cheley, S.; Bayley, H. *Nature* **1999**, *398*, 686-690.

(47) Gouaux, E. *Journal of Structural Biology* **1998**, *121*, 110-122.

(48) Braha, O.; Walker, B.; Cheley, S.; Kasianowicz, J. J.; Song, L. Z.; Gouaux, J. E.; Bayley, H. *Chemistry & Biology* **1997**, *4*, 497-505.

(49) Cheley, S.; Gu, L. Q.; Bayley, H. *Chemistry & Biology* **2002**, *9*, 829-838.

(50) Braha, O.; Gu, L. Q.; Zhou, L.; Lu, X. F.; Cheley, S.; Bayley, H. *Nature Biotechnology* **2000**, *18*, 1005-1007.

(51) Bayley, H.; Braha, O.; Gu, L. Q. *Advanced Materials* **2000**, *12*, 139-142.

(52) Johnson, S. J.; Bayerl, T. M.; McDermott, D. C.; Adam, G. W.; Rennie, A. R.; Thomas, R. K.; Sackmann, E. *Biophysical Journal* **1991**, *59*, 289-294.

(53) Lagerholm, B. C.; Starr, T. E.; Volovyk, Z. N.; Thompson, N. L. *Biochemistry* **2000**, *39*, 2042-2051.

(54) Cremer, P. S.; Boxer, S. G. *Journal of Physical Chemistry B* **1999**, *103*, 2554-2559.

(55) Zasadzinski, J. A. N.; Helm, C. A.; Longo, M. L.; Weisenhorn, A. L.; Gould, S. A. C.; Hansma, P. K. *Biophysical Journal* **1991**, *59*, 755-760.

(56) Egawa, H.; Furusawa, K. *Langmuir* **1999**, *15*, 1660-1666.

(57) Starr, T. E.; Thompson, N. L. *Langmuir* **2000**, *16*, 10301-10308.

(58) Ajo-Franklin, C. M.; Kam, L.; Boxer, S. G. *Proceedings of the National Academy of Sciences of the United States of America* **2001**, *98*, 13643-13648.

(59) Reimhult, E.; Hook, F.; Kasemo, B. *Langmuir* **2003**, *19*, 1681-1691.

(60) Stelzle, M.; Weissmuller, G.; Sackmann, E. *Journal of Physical Chemistry* **1993**, *97*, 2974-2981.

(61) Csucs, G.; Ramsden, J. J. *Biochimica Et Biophysica Acta-Biomembranes* **1998**, *1369*, 61-70.

(62) Yang, J. L.; Kleijn, J. M. *Biophysical Journal* **1999**, *76*, 323-332.

(63) Gritsch, S.; Nollert, P.; Jahnig, F.; Sackmann, E. *Langmuir* **1998**, *14*, 3118-3125.

(64) Bunjes, N.; Schmidt, E. K.; Jonczyk, A.; Rippmann, F.; Beyer, D.; Ringsdorf, H.; Graber, P.; Knoll, W.; Naumann, R. *Langmuir* **1997**, *13*, 6188-6194.

(65) Lahiri, J.; Kalal, P.; Frutos, A. G.; Jonas, S. T.; Schaeffler, R. *Langmuir* **2000**, *16*, 7805-7810.

(66) Salamon, Z.; Wang, Y.; Tollin, G.; Macleod, H. A. *Biochimica Et Biophysica Acta-Biomembranes* **1994**, *1195*, 267-275.

(67) Puu, G.; Gustafson, I. *Biochimica Et Biophysica Acta-Biomembranes* **1997**, *1327*, 149-161.

(68) Brian, A. A.; McConnell, H. M. *Proceedings of the National Academy of Sciences of the United States of America-Biological Sciences* **1984**, *81*, 6159-6163.

(69) McConnell, H. M.; Watts, T. H.; Weis, R. M.; Brian, A. A. *Biochimica Et Biophysica Acta* **1986**, *864*, 95-106.

(70) Kalb, E.; Frey, S.; Tamm, L. K. *Biochimica Et Biophysica Acta* **1992**, *1103*, 307-316.

(71) Langmuir, I. *Trans. Faraday Soc.* **1920**, *15*, 62-74.

(72) Petty, M. C. *Langmuir-Blodgett films: an introduction*; Cambridge: New York, 1996.

(73) Hope, M. J.; Bally, M. B.; Webb, G.; Cullis, P. R. *Biochimica Et Biophysica Acta* **1985**, *812*, 55-65.

(74) Mayer, L. D.; Hope, M. J.; Cullis, P. R. *Biochimica Et Biophysica Acta* **1986**, *858*, 161-168.

(75) Nayar, R.; Hope, M. J.; Cullis, P. R. *Biochimica Et Biophysica Acta* **1989**, *986*, 200-206.

(76) Frisken, B. J.; Asman, C.; Patty, P. J. *Langmuir* **2000**, *16*, 928-933.

(77) Barenholz, Y.; Gibbes, D.; Litman, B. J.; Goll, J.; Thompson, T. E.; Carlson, F. D. *Biochemistry* **1977**, *16*, 2806-2810.

(78) Mimms, L. T.; Zampighi, G.; Nozaki, Y.; Tanford, C.; Reynolds, J. A. *Biochemistry* **1981**, *20*, 833-840.

(79) Roessner, C. A.; Struck, D. K.; Ihler, G. M. *Journal of Biological Chemistry* **1983**, *258*, 643-648.

(80) Johnson, J. M.; Ha, T.; Chu, S.; Boxer, S. G. *Biophysical Journal* **2002**, *83*, 3371-3379.

(81) Stelzle, M.; Miehlich, R.; Sackmann, E. *Biophysical Journal* **1992**, *63*, 1346-1354.

(82) Fendler, J. H. *Chemistry of Materials* **2001**, *13*, 3196-3210.

(83) Holmlin, R. E.; Haag, R.; Chabinyc, M. L.; Ismagilov, R. F.; Cohen, A. E.; Terfort, A.; Rampi, M. A.; Whitesides, G. M. *Journal of the American Chemical Society* **2001**, *123*, 5075-5085.

(84) Ostuni, E.; Yan, L.; Whitesides, G. M. *Colloids and Surfaces B-Biointerfaces* **1999**, *15*, 3-30.

(85) Rao, N. M.; Plant, A. L.; Silin, V.; Wight, S.; Hui, S. W. *Biophysical Journal* **1997**, *73*, 3066-3077.

(86) Meuse, C. W.; Niaura, G.; Lewis, M. L.; Plant, A. L. *Langmuir* **1998**, *14*, 1604-1611.

(87) Rao, N. M.; Silin, V.; Ridge, K. D.; Woodward, J. T.; Plant, A. L. *Analytical Biochemistry* **2002**, *307*, 117-130.

(88) Langmuir, I.; Schaefer, V. J. *Journal of the American Chemical Society* **1938**, *60*, 1351-1360.

(89) Hubbard, J. B.; Silin, V.; Plant, A. L. *Biophysical Chemistry* **1998**, *75*, 163-176.

(90) Peng, Z. Q.; Tang, J. L.; Han, X. J.; Wang, E. K.; Dong, S. J. *Langmuir* **2002**, *18*, 4834-4839.

(91) Meuse, C. W.; Krueger, S.; Majkrzak, C. F.; Dura, J. A.; Fu, J.; Connor, J. T.; Plant, A. L. *Biophysical Journal* **1998**, *74*, 1388-1398.

(92) Plant, A. L.; Gueguetchkeri, M.; Yap, W. *Biophysical Journal* **1994**, *67*, 1126-1133.

(93) Kastl, K.; Ross, M.; Gerke, V.; Steinem, C. *Biochemistry* **2002**, *41*, 10087-10094.

(94) Glazier, S. A.; Vanderah, D. J.; Plant, A. L.; Bayley, H.; Valincius, G.; Kasianowicz, J. J. *Langmuir* **2000**, *16*, 10428-10435.

(95) Krueger, S.; Meuse, C. W.; Majkrzak, C. F.; Dura, J. A.; Berk, N. F.; Tarek, M.; Plant, A. L. *Langmuir* **2001**, *17*, 511-521.

(96) Wong, J. Y.; Majewski, J.; Seitz, M.; Park, C. K.; Israelachvili, J. N.; Smith, G. S. *Biophysical Journal* **1999**, *77*, 1445-1457.

(97) Wagner, M. L.; Tamm, L. K. *Biophysical Journal* **2000**, *79*, 1400-1414.

(98) Hillebrandt, H.; Wiegand, G.; Tanaka, M.; Sackmann, E. *Langmuir* **1999**, *15*, 8451-8459.

(99) Majewski, J.; Wong, J. Y.; Park, C. K.; Seitz, M.; Israelachvili, J. N.; Smith, G. S. *Biophysical Journal* **1998**, *75*, 2363-2367.

(100) Ma, C.; Srinivasan, M. P.; Waring, A. J.; Lehrer, R. I.; Longo, M. L.; Stroeve, P. *Colloids and Surfaces B-Biointerfaces* **2003**, *28*, 319-329.

(101) Kugler, R.; Knoll, W. *Bioelectrochemistry* **2002**, *56*, 175-178.

(102) Wong, J. Y.; Park, C. K.; Seitz, M.; Israelachvili, J. *Biophysical Journal* **1999**, *77*, 1458-1468.

(103) Onda, M.; Lvov, Y.; Ariga, K.; Kunitake, T. *Japanese Journal of Applied Physics Part 2-Letters* **1997**, *36*, L1608-L1611.

(104) Wagner, M. L.; Tamm, L. K. *Biophysical Journal* **2001**, *81*, 266-275.

(105) Albertorio, F.; Diaz, A. J.; Yang, T. L.; Chapa, V. A.; Kataoka, S.; Castellana, E. T.; Cremer, P. S. *Langmuir* **2005**, *21*, 7476-7482.

(106) Harada, H.; Ueda, T. *Chemical Physics Letters* **1984**, *106*, 229-231.

(107) Ding, X. Z.; Qi, Z. Z.; He, Y. Z. *Journal of Materials Science Letters* **1995**, *14*, 21-22.

(108) Montoya, I. A.; Viveros, T.; Dominguez, J. M.; Canales, L. A.; Schifter, I. *Catalysis Letters* **1992**, *15*, 207-217.

(109) Barringer, E. A.; Bowen, H. K. *Journal of the American Ceramic Society* **1982**, *65*, C199-C201.

(110) Kataoka, S.; Gurau, M. C.; Albertorio, F.; Holden, M. A.; Lim, S. M.; Yang, R. D.; Cremer, P. S. *Langmuir* **2004**, *20*, 1662-1666.

(111) Nishimoto, S.; Ohtani, B.; Shirai, H.; Kagiya, T. *Journal of the Chemical Society-Perkin Transactions 2* **1986**, 661-665.

(112) Kaneko, M.; I., O., Eds. *Photocatalysis: Science and Technology*; Springer: New York, 2002.

(113) Chan, S. C.; Barteau, M. A. *Langmuir* **2005**, *21*, 5588-5595.

(114) Chang, F. W.; Yu, H. Y.; Roselin, L. S.; Yang, H. C. *Applied Catalysis a-General* **2005**, *290*, 138-147.

(115) Isono, R.; Yoshimura, T.; Esumi, K. *Journal of Colloid and Interface Science* **2005**, *288*, 177-183.

(116) Chou, J.; McFarland, E. W. *Chemical Communications* **2004**, 1648-1649.

(117) Tada, H.; Ishida, T.; Takao, A.; Ito, S.; Mukhopadhyay, S.; Akita, T.; Tanaka, K.; Kobayashi, H. *Chemphyschem* **2005**, *6*, 1537-1543.

(118) Naoi, K.; Ohko, Y.; Tatsuma, T. *Chemical Communications* **2005**, 1288-1290.

(119) Grunert, W.; Bruckner, A.; Hofmeister, H.; Claus, P. *Journal of Physical Chemistry B* **2004**, *108*, 5709-5717.

(120) Park, H.; Choi, W. *Catalysis Today* **2005**, *101*, 291-297.

(121) Marinkovic, S.; Hoffmann, N. *European Journal of Organic Chemistry* **2004**, 3102-3107.

(122) Ho, W. K.; Yu, J. C.; Yu, J. G. *Langmuir* **2005**, *21*, 3486-3492.

(123) Zhang, L. F.; Kanki, T.; Sano, N.; Toyoda, A. *Separation and Purification Technology* **2003**, *31*, 105-110.

(124) Ilisz, I.; Dombi, A.; Mogyorosi, K.; Farkas, A.; Dekany, I. *Applied Catalysis B-Environmental* **2002**, *39*, 247-256.

(125) Vautier, M.; Guillard, C.; Herrmann, J. M. *Journal of Catalysis* **2001**, *201*, 46-59.

(126) Krishna, V.; Pumprueg, S.; Lee, S. H.; Zhao, J.; Sigmund, W.; Koopman, B.; Moudgil, B. M. *Process Safety and Environmental Protection* **2005**, *83*, 393-397.

(127) Yu, M. J.; Kim, B. W. *Journal of Microbiology and Biotechnology* **2004**, *14*, 1105-1113.

(128) Sokmen, M.; Candan, F.; Sumer, Z. *Journal of Photochemistry and Photobiology a-Chemistry* **2001**, *143*, 241-244.

(129) Woolley, A. T.; Mathies, R. A. *Analytical Chemistry* **1995**, *67*, 3676-3680.

(130) Simpson, P. C.; Roach, D.; Woolley, A. T.; Thorsen, T.; Johnston, R.; Sensabaugh, G. F.; Mathies, R. A. *Proceedings of the National Academy of Sciences of the United States of America* **1998**, *95*, 2256-2261.

(131) Liu, S. R.; Shi, Y. N.; Ja, W. W.; Mathies, R. A. *Analytical Chemistry* **1999**, *71*, 566-573.

(132) Kopp, M. U.; de Mello, A. J.; Manz, A. *Science* **1998**, *280*, 1046-1048.

(133) Waters, L. C.; Jacobson, S. C.; Kroutchinina, N.; Khandurina, J.; Foote, R. S.; Ramsey, J. M. *Analytical Chemistry* **1998**, *70*, 5172-5176.

(134) Burns, M. A.; Johnson, B. N.; Brahmasandra, S. N.; Handique, K.; Webster, J. R.; Krishnan, M.; Sammarco, T. S.; Man, P. M.; Jones, D.; Heldsinger, D.; Mastrangelo, C. H.; Burke, D. T. *Science* **1998**, *282*, 484-487.

(135) Cheng, J.; Waters, L. C.; Fortina, P.; Hvichia, G.; Jacobson, S. C.; Ramsey, J. M.; Kricka, L. J.; Wilding, P. *Analytical Biochemistry* **1998**, *257*, 101-106.

(136) Northrup, M. A.; Benett, B.; Hadley, D.; Landre, P.; Lehew, S.; Richards, J.; Stratton, P. *Analytical Chemistry* **1998**, *70*, 918-922.

(137) Lauks, I. R. *Accounts of Chemical Research* **1998**, *31*, 317-324.

(138) Peled, N. *Pure and Applied Chemistry* **1996**, *68*, 1837-1841.

(139) Chiem, N.; Harrison, D. J. *Analytical Chemistry* **1997**, *69*, 373-378.

(140) Colyer, C. L.; Tang, T.; Chiem, N.; Harrison, D. J. *Electrophoresis* **1997**, *18*, 1733-1741.

(141) Kricka, L. J.; Wilding, P. *Pure and Applied Chemistry* **1996**, *68*, 1831-1836.

(142) Braxton, S.; Bedilion, T. *Current Opinion in Biotechnology* **1998**, *9*, 643-649.

(143) Yamaguchi, A.; Jin, P.; Tsuchiyama, H.; Masuda, T.; Sun, K.; Matsuo, S.; Misawa, H. *Analytica Chimica Acta* **2002**, *468*, 143-152.

(144) Holden, M. A.; Jung, S. Y.; Cremer, P. S. *Analytical Chemistry* **2004**, *76*, 1838-1843.

(145) Delamarche, E.; Bernard, A.; Schmid, H.; Michel, B.; Biebuyck, H. *Science* **1997**, *276*, 779-781.

(146) Chiu, D. T.; Jeon, N. L.; Huang, S.; Kane, R. S.; Wargo, C. J.; Choi, I. S.; Ingber, D. E.; Whitesides, G. M. *Proceedings of the National Academy of Sciences of the United States of America* **2000**, *97*, 2408-2413.

(147) Chiem, N. H.; Harrison, D. J. *Electrophoresis* **1998**, *19*, 3040-3044.

(148) Vandenberg, A.; Grisel, A.; Verneynorberg, E.; Vanderschoot, B. H.; Koudelkahep, M.; Derooij, N. F. *Sensors and Actuators B-Chemical* **1993**, *13*, 396-399.

(149) Santini, J. T.; Cima, M. J.; Langer, R. *Nature* **1999**, *397*, 335-338.

(150) Effenhauser, C. S.; Bruin, G. J. M.; Paulus, A.; Ehrat, M. *Analytical Chemistry* **1997**, *69*, 3451-3457.

(151) Chou, H. P.; Spence, C.; Scherer, A.; Quake, S. *Proceedings of the National Academy of Sciences of the United States of America* **1999**, *96*, 11-13.

(152) Duffy, D. C.; McDonald, J. C.; Schueller, O. J. A.; Whitesides, G. M. *Analytical Chemistry* **1998**, *70*, 4974-4984.

(153) Xia, Y. N.; McClelland, J. J.; Gupta, R.; Qin, D.; Zhao, X. M.; Sohn, L. L.; Celotta, R. J.; Whitesides, G. M. *Advanced Materials* **1997**, *9*, 147-149.

(154) Qin, D.; Xia, Y. N.; Whitesides, G. M. *Advanced Materials* **1996**, *8*, 917-&.

(155) Xia, Y. N.; Tien, J.; Qin, D.; Whitesides, G. M. *Langmuir* **1996**, *12*, 4033-4038.

(156) Wilbur, J. L.; Kumar, A.; Kim, E.; Whitesides, G. M. *Advanced Materials* **1994**, *6*, 600-604.

(157) Mrksich, M.; Whitesides, G. M. *Trends in Biotechnology* **1995**, *13*, 228-235.

(158) Xia, Y. N.; Mrksich, M.; Kim, E.; Whitesides, G. M. *Journal of the American Chemical Society* **1995**, *117*, 9576-9577.

(159) Wilbur, J. L.; Kumar, A.; Biebuyck, H. A.; Kim, E.; Whitesides, G. M. *Nanotechnology* **1996**, *7*, 452-457.

(160) Mrksich, M.; Dike, L. E.; Tien, J.; Ingber, D. E.; Whitesides, G. M. *Experimental Cell Research* **1997**, *235*, 305-313.

(161) McDonald, J. C.; Duffy, D. C.; Anderson, J. R.; Chiu, D. T.; Wu, H. K.; Schueller, O. J. A.; Whitesides, G. M. *Electrophoresis* **2000**, *21*, 27-40.

(162) Lee, J. N.; Park, C.; Whitesides, G. M. *Analytical Chemistry* **2003**, *75*, 6544-6554.

(163) Kendall, D. L. *Applied Physics Letters* **1975**, *26*, 195-198.

(164) Rogers, T.; Kowal, J. *Sensors and Actuators a-Physical* **1995**, *46*, 113-120.

(165) Caelen, I.; Bernard, A.; Juncker, D.; Michel, B.; Heinzelmann, H.; Delamarche, E. *Langmuir* **2000**, *16*, 9125-9130.

(166) Barker, S. L. R.; Tarlov, M. J.; Canavan, H.; Hickman, J. J.; Locascio, L. E. *Analytical Chemistry* **2000**, *72*, 4899-4903.

(167) Delamarche, E.; Bernard, A.; Schmid, H.; Bietsch, A.; Michel, B.; Biebuyck, H. *Journal of the American Chemical Society* **1998**, *120*, 500-508.

(168) Su, J.; Bringer, M. R.; Ismagilov, R. F.; Mrksich, M. *Journal of the American Chemical Society* **2005**, *127*, 7280-7281.

(169) Cesaro-Tadic, S.; Dernick, G.; Juncker, D.; Buurman, G.; Kropshofer, H.; Michel, B.; Fattinger, C.; Delamarche, E. *Lab on a Chip* **2004**, *4*, 563-569.

(170) Khademhosseini, A.; Suh, K. Y.; Jon, S.; Eng, G.; Yeh, J.; Chen, G. J.; Langer, R. *Analytical Chemistry* **2004**, *76*, 3675-3681.

(171) Jiang, X. Y.; Ng, J. M. K.; Stroock, A. D.; Dertinger, S. K. W.; Whitesides, G. M. *Journal of the American Chemical Society* **2003**, *125*, 5294-5295.

(172) Kenis, P. J. A.; Ismagilov, R. F.; Whitesides, G. M. *Science* **1999**, *285*, 83-85.

(173) Huck, W. T. S.; Yan, L.; Stroock, A.; Haag, R.; Whitesides, G. M. *Langmuir* **1999**, *15*, 6862-6867.

(174) Korchev, A. S.; Bozack, M. J.; Slaten, B. L.; Mills, G. *Journal of the American Chemical Society* **2004**, *126*, 10-11.

(175) Baldacchini, T.; Pons, A. C.; Pons, J.; LaFratta, C. N.; Fourkas, J. T.; Sun, Y.; Naughton, M. J. *Optics Express* **2005**, *13*, 1275-1280.

(176) Li, S. L.; Macosko, C. W.; White, H. S. *Science* **1993**, *259*, 957-960.

(177) Takayama, S.; McDonald, J. C.; Ostuni, E.; Liang, M. N.; Kenis, P. J. A.; Ismagilov, R. F.; Whitesides, G. M. *Proceedings of the National Academy of Sciences of the United States of America* **1999**, *96*, 5545-5548.

(178) Hoffmann, M. R.; Martin, S. T.; Choi, W. Y.; Bahnemann, D. W. *Chemical Reviews* **1995**, *95*, 69-96.

(179) Shchukin, D.; Ustinovich, E.; Sviridov, D.; Pichat, P. *Photochemical & Photobiological Sciences* **2004**, *3*, 142-144.

(180) Szabo-Bardos, E.; Czili, H.; Horvath, A. *Journal of Photochemistry and Photobiology a-Chemistry* **2003**, *154*, 195-201.

(181) Sahyun, M. R. V.; Serpone, N. *Langmuir* **1997**, *13*, 5082-5088.

(182) Fleischauer, P. D.; Shepherd, J. R.; Kan, H. K. A. *Journal of the American Chemical Society* **1972**, *94*, 283-&.

(183) Litter, M. I. *Applied Catalysis B-Environmental* **1999**, *23*, 89-114.

(184) Nishimoto, S.; Ohtani, B.; Kajiwara, H.; Kagiya, T. *Journal of the Chemical Society-Faraday Transactions I* **1983**, *79*, 2685-2694.

(185) Zhang, F. X.; Guan, N. J.; Li, Y. Z.; Zhang, X.; Chen, J. X.; Zeng, H. S. *Langmuir* **2003**, *19*, 8230-8234.

(186) Ikeda, S.; Akamatsu, K.; Nawafune, H. *Journal of Materials Chemistry* **2001**, *11*, 2919-2921.

(187) Fadeev, A. Y.; McCarthy, T. J. *Journal of the American Chemical Society* **1999**, *121*, 12184-12185.

(188) Fadeev, A. Y.; McCarthy, T. J. *Langmuir* **1999**, *15*, 3759-3766.

(189) Remillard, J. T.; McBride, J. R.; Nietering, K. E.; Drews, A. R.; Zhang, X. *Journal of Physical Chemistry B* **2000**, *104*, 4440-4447.

(190) Alvarez-Herrero, A.; Fort, A. J.; Guerrero, H.; Bernabeu, E. *Thin Solid Films* **1999**, *349*, 212-219.

(191) Ohtani, B.; Okugawa, Y.; Nishimoto, S.; Kagiya, T. *Journal of Physical Chemistry* **1987**, *91*, 3550-3555.

(192) Kambe, S.; Nakade, S.; Wada, Y.; Kitamura, T.; Yanagida, S. *Journal of Materials Chemistry* **2002**, *12*, 723-728.

(193) Warman, J. M.; Dehaas, M. P.; Gratzel, M.; Infelta, P. P. *Nature* **1984**, *310*, 306-308.

(194) Colombo, D. P.; Bowman, R. M. *Journal of Physical Chemistry* **1995**, *99*, 11752-11756.

(195) Mao, H. B.; Yang, T. L.; Cremer, P. S. *Journal of the American Chemical Society* **2002**, *124*, 4432-4435.

(196) Santra, A. K.; Yang, F.; Goodman, D. W. *Surface Science* **2004**, *548*, 324-332.

(197) He, J. H.; Ichinose, I.; Kunitake, T.; Nakao, A.; Shiraishi, Y.; Toshima, N. *Journal of the American Chemical Society* **2003**, *125*, 11034-11040.

(198) Tokareva, I.; Minko, S.; Fendler, J. H.; Hutter, E. *Journal of the American Chemical Society* **2004**, *126*, 15950-15951.

(199) Lahav, M.; Vaskevich, A.; Rubinstein, I. *Langmuir* **2004**, *20*, 7365-7367.

(200) Hutter, E.; Pileni, M. P. *Journal of Physical Chemistry B* **2003**, *107*, 6497-6499.

(201) Kalyuzhny, G.; Schneeweiss, M. A.; Shanzer, A.; Vaskevich, A.; Rubinstein, I. *Journal of the American Chemical Society* **2001**, *123*, 3177-3178.

(202) Geddes, C. D.; Parfenov, A.; Roll, D.; Fang, J. Y.; Lakowicz, J. R. *Langmuir* **2003**, *19*, 6236-6241.

(203) Sokolov, K.; Chumanov, G.; Cotton, T. M. *Analytical Chemistry* **1998**, *70*, 3898-3905.

(204) Attridge, J. W.; Daniels, P. B.; Deacon, J. K.; Robinson, G. A.; Davidson, G. P. *Biosensors & Bioelectronics* **1991**, *6*, 201-214.

(205) Moran-Mirabal, J. M.; Edel, J. B.; Meyer, G. D.; Throckmorton, D.; Singh, A. K.; Craighead, H. G. *Biophysical Journal* **2005**, *89*, 296-305.

(206) Poulsen, C. R.; Culbertson, C. T.; Jacobson, S. C.; Ramsey, J. M. *Analytical Chemistry* **2005**, *77*, 667-672.

(207) Yang, T.; Baryshnikova, O. K.; Mao, H. B.; Holden, M. A.; Cremer, P. S. *Journal of the American Chemical Society* **2003**, *125,* 4779-4784.

(208) Kung, L. A.; Groves, J. T.; Ulman, N.; Boxer, S. G. *Advanced Materials* **2000**, *12*, 731-+.

(209) Yang, T. L.; Simanek, E. E.; Cremer, P. *Analytical Chemistry* **2000**, *72*, 2587-2589.

(210) Yamazaki, V.; Sirenko, O.; Schafer, R. J.; Nguyen, L.; Gutsmann, T.; Brade, L.; Groves, J. T. *Bmc Biotechnology* **2005**, *5*.

(211) Sapuri, A. R.; Baksh, M. M.; Groves, J. T. *Langmuir* **2003**, *19*, 1606-1610.

(212) Hovis, J. S.; Boxer, S. G. *Langmuir* **2001**, *17*, 3400-3405.

(213) Kung, L. A.; Kam, L.; Hovis, J. S.; Boxer, S. G. *Langmuir* **2000**, *16*, 6773-6776.

(214) Tamm, L. K. In *Optical Microscopy: Emerging Methods and Applications*; Herman, B., Lemasters, J. J., Ed.; Academic Press, Inc.: San Diego, 1993, pp 295-337.

(215) Yee, C. K.; Amweg, M. L.; Parikh, A. N. *Journal of the American Chemical Society* **2004**, *126*, 13962-13972.

(216) Morigaki, K.; Baumgart, T.; Offenhausser, A.; Knoll, W. *Angewandte Chemie-International Edition* **2001**, *40*, 172-174.

(217) Ilic, B.; Craighead, H. G. *Biomedical Microdevices* **2000**, *2*, 317 - 322.

(218) Ratzlaff, E. H.; Grinvald, A. *Journal of Neuroscience Methods* **1991**, *36*, 127-137.

(219) Sasaki, S.; Yazawa, I.; Miyakawa, N.; Mochida, H.; Shinomiya, K.; Kamino, K.; Momose-Sato, Y.; Sato, K. *Neuroimage* **2002**, *17*, 1240-1255.

(220) Vanzetta, I.; Grinvald, A. *Science* **1999**, *286*, 1555-1558.

(221) Lefkowitz, L. *The Manual of Close-Up Photography*; American Photographic Book Publishing: New York, 1979.

(222) Toomre, D.; Manstein, D. J. *Trends in Cell Biology* **2001**, *11*, 298-303.

(223) Bayley, H.; Cremer, P. S. *Nature* **2001**, *413*, 226-230.

(224) Stryer, L. *Annual Review of Biochemistry* **1978**, *47*, 819-846.

(225) Morris, A. J.; Malbon, C. C. *Physiological Reviews* **1999**, *79*, 1373-1430.

(226) Li, E.; Hristova, K. *Langmuir* **2004**, *20*, 9053-9060.

(227) Parthasarathy, R.; Jackson, B. L.; Lowery, T. J.; Wong, A. P.; Groves, J. T. *Journal of Physical Chemistry B* **2004**, *108*, 649-657.

(228) Wolf, D. E.; Winiski, A. P.; Ting, A. E.; Bocian, K. M.; Pagano, R. E. *Biochemistry* **1992**, *31*, 2865-2873.

(229) Kim, E. E.; Wyckoff, H. W. *Journal of Molecular Biology* **1991**, *218*, 449-464.

(230) Tamm, L. K.; Bartoldus, I. *Biochemistry* **1988**, *27*, 7453-7458.

(231) Mammen, M.; Choi, S. K.; Whitesides, G. M. *Angewandte Chemie-International Edition* **1998**, *37*, 2755-2794.

(232) Min, H. S.; Joo, Y. C.; Song, O. S. *Journal of Electronic Packaging* **2004**, *126*, 120-123.

VITA

Name:	Edward Thomas Castellana
Address:	128 Gardner St Fredonia, NY 14063
Email Address:	castellana@mail.chem.tamu.edu
Education:	B.S., Mathematical Physics and Chemistry, State University of New York College at Fredonia, 1999